1999

Frontogenesis in the North Pacific Oceanic Frontal Zones--A Numerical Simulation

Michael S. Dinniman
Old Dominion University, msd@ccpo.odu.edu

Michele M. Rienecker

Original Publication Citation

Dinniman, M.S., & Rienecker, M.M. (1999). Frontogenesis in the North Pacific oceanic frontal zones--A numerical simulation. *Journal of Physical Oceanography, 29*(4), 537-559. doi: 10.1175/1520-0485(1999)0292.0.co;2

Frontogenesis in the North Pacific Oceanic Frontal Zones—A Numerical Simulation

MICHAEL S. DINNIMAN

Hughes STX, Lanham, Maryland

MICHELE M. RIENECKER

Oceans and Ice Branch, Laboratory for Hydrospheric Processes, NASA/Goddard Space Flight Center, Greenbelt, Maryland

(Manuscript received 2 July 1997, in final form 20 April 1998)

ABSTRACT

A primitive equation model [Geophysical Fluid Dynamics Laboratory's (GFDL's) MOM 2] with one degree horizontal resolution is used to simulate the seasonal cycle of frontogenesis in the subarctic frontal zone (SAFZ) and the subtropical frontal zone (STFZ) of the North Pacific Ocean. The SAFZ in the model contains deep (greater than 500 m in some places) regions with seasonally varying high gradients in temperature and salinity. The gradients generally weaken toward the east. The STFZ consists of a relatively shallow (less than 200 m in most places) region of high gradient in temperature that disappears in the summer/fall. The high gradient in salinity in the STFZ maintains its strength year round and extends across almost the entire basin. The model simulates the location and intensity of the frontal zones in good agreement with climatological observations: generally to within two degrees of latitude and usually at the same or slightly stronger intensity. The seasonal cycle of the frontal zones also matches observations well, although the subarctic front is stronger than observed in winter and spring.

The model balances are examined to identify the dominant frontogenetic processes. The seasonal cycle of temperature frontogenesis in the surface level of the model is governed by both the convergence of the wind-driven Ekman transport and differential heating/cooling. In the STFZ, the surface Ekman convergence is frontogenetic throughout the year as opposed to surface heating, which is frontogenetic during winter and strongly frontolytic during late spring and summer. The subarctic front at 40°N in the central Pacific (not the maximum wintertime gradient in the model, but its location in summer and the location where variability is in best agreement with the observations) undergoes frontogenesis during spring and summer due to surface Ekman convergence and differential horizontal shear. The frontolysis during winter is due to the joint influence of differential heat flux and vertical convection in opposition to frontogenetic Ekman convergence. The seasonal cycle of salinity frontogenesis in the surface level is governed by Ekman convergence, differential surface freshwater flux, and differential vertical convection (mixing). For salinity, the differential convection is primarily forced by Ekman convergence and differential cooling, thereby linking the salinity and temperature frontogenesis/frontolysis. Below the surface level, the seasonal frontogenesis/frontolysis is only significant in the western and central SAFZ where it is due primarily to differential mixing (mostly in winter and early spring) with contributions from convergence and shearing advection during fall and winter. The shearing advection in the model western SAFZ is likely a result of the Kuroshio overshooting its observed separation latitude. The model's vertical mixing through convective adjustment is found to be very important in controlling much of the frontogenesis/frontolysis. Thus, the seasonal cycle of the surface frontal variability depends strongly on the subsurface structure.

1. Introduction

The North Pacific Ocean is traversed by the subarctic–subtropical transition zone that separates the cold, fresh surface water of the subarctic gyre from the warm, saline surface water of the subtropical gyre. The northern and southern boundaries of this zone are large-scale oceanic frontal zones (OFZs) that can exhibit rapid meridional changes in thermohaline structure, hydrostatic stability structure, and biological species composition (Roden 1991). The northern boundary is referred to as the subarctic frontal zone (SAFZ) and the southern boundary as the subtropical frontal zone (STFZ). Synoptic surveys within the OFZs reveal several sharp temperature and salinity fronts embedded within the broader fronts (Roden 1977, 1980a; Niiler and Reynolds 1984). The location of the strongest gradient changes from survey to survey so that the resultant long-term climatology displays mean fronts that are broader and weaker than the synoptic fronts. This paper is concerned with seasonal variations of the large-scale North Pacific OFZs; here

Corresponding author address: Michael S. Dinniman, Old Dominion University, Ctr. Coastal Physical Oceanography, Crittenton Hall, Norfolk, VA 23529.
E-mail: msd@ccpo.odu.edu

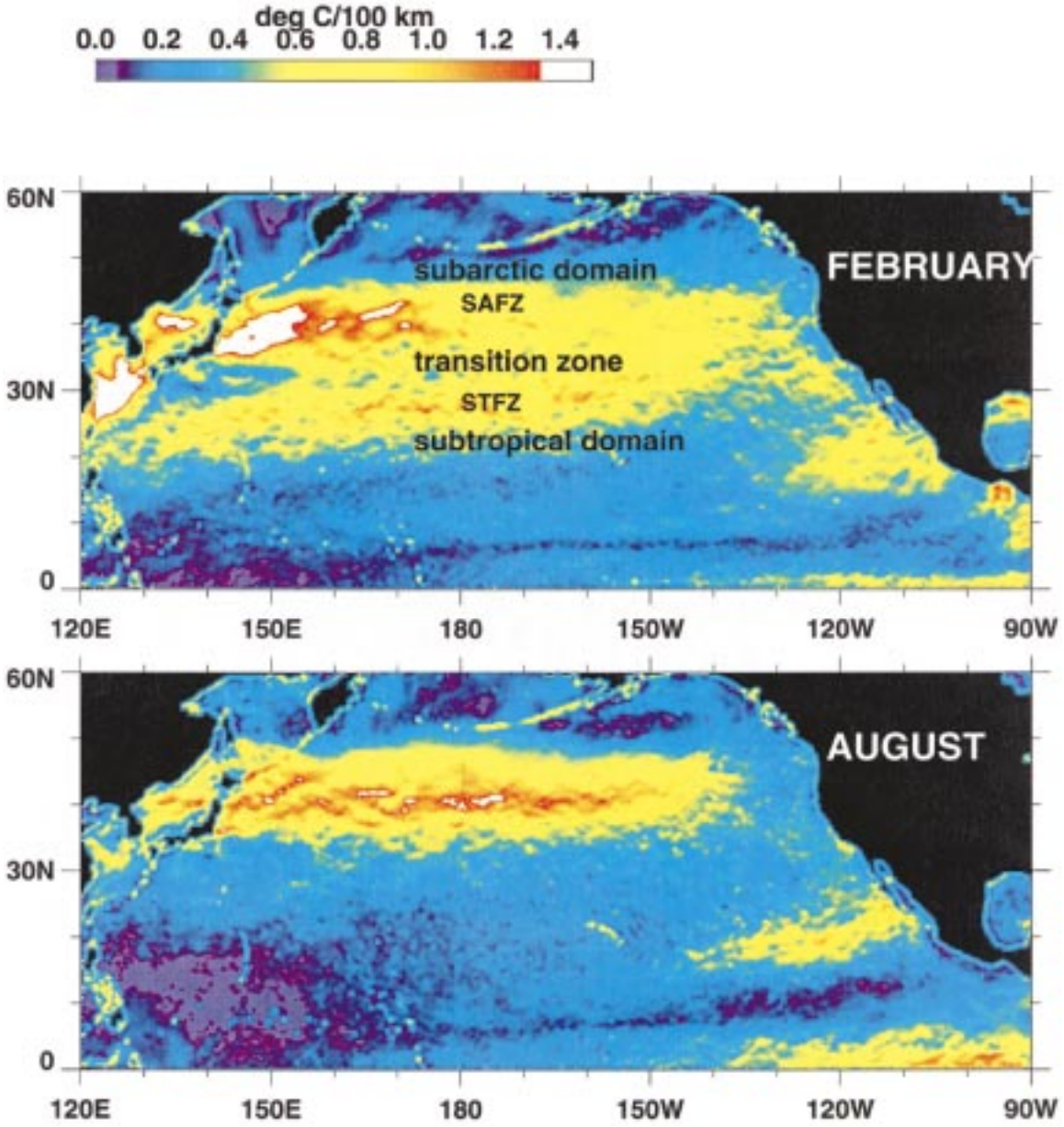

FIG. 1. Magnitude of the horizontal gradient of monthly sea surface temperature climatology from AVHRR MCSST data for February and August.

the term ''front'' will refer to the broader climatological front in an OFZ unless explicitly stated otherwise.

The large-scale OFZs are readily apparent in images of the gradient of the sea surface temperature over the North Pacific from a monthly climatology of 11 years of multichannel sea surface temperature (MCSST) from Advanced Very High Resolution Radiometer (AVHRR) data (Smith 1992) for February and August (Fig. 1). The broad frontal region associated with the meandering Oyashio and Kuroshio Extension is clearly seen in the western basin between 35° and 40°N. Near 160°E, the Kuroshio Extension bifurcates and the more northern, stronger front becomes what Levine and White (1983) term the Northern Subarctic Front and Zhang and Hanawa (1993) term the Kuroshio Bifurcation Front (KBF).

The SAFZ is primarily zonally oriented and is located between 40° and 43°N in the central Pacific. The southern limit is often defined by the outcrop of the 33.8 psu isohaline that forms the bottom of the halocline in the subarctic ocean (Lynn 1986; Roden 1991). The northern limit can be defined by the outcrop of the 33.0 psu isohaline, which lies near the top of the subarctic halocline. The location does not change much seasonally although variations have been found in the strength of

the temperature front (Roden 1980b; Kazmin and Rienecker 1996, henceforth referred to as KR). From AVHRR data (Fig. 1), the gradients are stronger in the western basin during winter and stronger in the central Pacific during summer. In the SAFZ, the horizontal temperature and salinity gradients tend to compensate each other so that the resulting density gradients are weak (Roden 1972, 1975, 1977).

The STFZ is also primarily zonally oriented and is located near 30°N in the central Pacific. The northern limit can be described by a thermohaline front in winter in which the 34.8 psu isohaline and 18°C isotherm are embedded (Roden 1980a). The southern limit can be defined by the outcrop of the 35.2 psu isohaline, which lies near the top of the subtropical halocline. The density gradient is also weak in the STFZ (Niiler and Reynolds 1984) and the front is primarily a salinity front in the upper layer (Roden 1991). The STFZ has a much stronger seasonal cycle than the SAFZ with the surface temperature front practically disappearing in summer and only the salinity front being evident at the surface (White et al. 1978).

There are four primary physical processes responsible for frontogenesis (e.g., Roden 1991): differential horizontal advection of temperature and salinity, particularly that associated with surface Ekman transport; differential vertical advection of temperature and salinity, particularly as associated with Ekman pumping; differential radiative heat and freshwater fluxes; and differential turbulent heat and salt (or freshwater) fluxes.

Ekman convergence was often assumed in early studies to be the primary dynamical mechanism acting in the OFZs. Roden and Paskausky (1978) were able to estimate patterns of frontogenesis and frontolysis in the STFZ in winter using a simple model based on Ekman dynamics with one degree horizontal resolution but only over timescales of a week or less. Camerlengo (1982) used a four-layer hydrodynamical model of the SAFZ to show that the effect of a negative wind stress curl is to produce convergence at the front, strongly favoring frontogenesis. However, many recent studies have identified other possible mechanisms in addition to Ekman transport convergence for the formation and maintenance of both frontal zones. In a numerical simulation study using a two-dimensional bulk mixed-layer model, Cushman-Roisin (1981) showed that differential vertical mixing is as efficient as horizontal advection for large-scale ocean frontogenesis. Kazmin and Rienecker (1996), in an analysis of MCSST with satellite-derived wind products and heat flux estimates based on the Comprehensive Ocean–Atmosphere Data Set (COADS), showed that most of the observed frontogenesis variability in the North Pacific OFZs on seasonal timescales is explained by the combined forcing due to wind stress and net surface heat flux. In their study, the primary source of seasonal variability in meridional frontogenesis was found to be the meridional gradient of the net surface heat flux, which sometimes opposed the frontogenetic tendencies due to Ekman convergence.

Cushman-Roisin (1984) demonstrated that, given the thermally driven flow, convergence due to beta plane dynamics could contribute to the formation and maintainance of the Subtropical Front. Takeuchi (1984, 1986) was able to spin up a realistic subtropical front and countercurrent (the shallow eastward density-driven geostrophic flow associated with the subtropical front) under the influence of meridional variations in zonal wind stress and surface buoyancy flux. He used a primitive equation model with a resolution of 320 km zonally and 160 km meridionally. Seasonal variations in the surface forcing produced realistic seasonal variations in the structure of the front. He concluded that the seasonal variation of the countercurrent was primarily due to the seasonal variability in the wind stress. The seasonal buoyancy flux intensified the annual mean gradient because of the asymmetrical effects of buoyancy sources (shallow) and sinks (deep because of convection).

In a study of the SAFZ in the central North Pacific, Roden (1977) suggested that the frontogenesis depended strongly on differential horizontal and vertical Ekman advection and the existing vertical and horizontal thermohaline gradients. Yuan and Talley (1996) performed a study of the SAFZ using the Levitus (1982) climatological data and several conductivity–temperature–depth probe/profiler–salinity, temperature, and depth probe (CTD–STD) sections highlighting the seasonal variations of the climatological frontal zone and the structure of the frontal zone in synoptic surveys. They could not identify a specific frontogenetic mechanism for the mean SAFZ and hypothesized that the subarctic front is initiated at the Oyashio front in the western North Pacific and advected across the North Pacific by the North Pacific Current and the Subarctic Current. In another study of the SAFZ, Yuan (1994), using surface wind velocities from the Fleet Numerical Oceanography Center and CTD/STD sections, concluded that the seasonal Ekman convergence contributes to SAFZ frontogenesis but the annual mean does not.

In this study, a finite difference primitive equation model is used to simulate the circulation of the North Pacific Ocean. The model configuration is described in section 2. The model's representation of the large-scale frontal zones is described in section 3. It is validated against observations there and in section 4, where the relative contributions of various dynamic and thermodynamic processes to seasonal frontogenesis/frontolysis in the OFZ are examined. Finally, the results are compared with those from other studies and the different mechanisms contributing to frontogenesis/frontolysis are discussed in section 5.

2. Model configuration

The Modular Ocean Model (MOM 2, see Pacanowski 1995) developed at the Geophysical Fluid Dynamics

Laboratory was used for this study. The model domain extends from 10°S to 64°N and includes realistic ocean bathymetry. The northern and southern boundaries were treated as solid walls with no heat or salt flux across the boundaries and a no-slip condition for momentum. The model was run in spherical coordinates with a 1° horizontal resolution and 18 vertical levels of varying thickness. The vertical levels were concentrated in the upper ocean with nine levels in the upper 200 m (5, 25, 50, 75, 100, 125, 150, 175, 200, 250, 300, 350, 400, 500, 700, 1000, 2000, and 4000 m). The model equations governing the time rate of change of the temperature T and salinity S are

$$T_t + \mathcal{L}(T) = \kappa_h T_{zz} + A_h \nabla^2 T,$$

$$S_t + \mathcal{L}(S) = \kappa_h S_{zz} + A_h \nabla^2 S,$$

where $\mathcal{L}(\alpha)$ is the advection operator

$$\mathcal{L}(\alpha) = \frac{1}{a \cos\phi}[(u\alpha)_\lambda + (v\alpha \cos\phi)_\phi] + (w\alpha)_z;$$

here, ∇^2 is the horizontal Laplacian; the subscript denotes differentation; λ is longitude; ϕ is latitude; z is height relative to the earth's mean radius a (measured positive upwards); and (u, v, w) are the zonal, meridional, and vertical velocities. For vertical mixing of tracers and momentum, $\kappa_h = 3.0 \times 10^{-5}$ m^2 s^{-1} and $\kappa_m = 2.0 \times 10^{-3}$ m^2 s^{-1}; for horizontal mixing of tracers and momentum, $A_h = 2.0 \times 10^2$ m^2 s^{-1} and $A_m = 2.5 \times 10^4$ m^2 s^{-1}. The model was run with an explicit convection scheme and the rigid-lid approximation. There is no explicit mixed layer formulation; surface mixing processes are incorporated only through the applied vertical diffusion and convective overturning.

The model was initialized with the Levitus temperature and salinity climatology (Levitus 1982) and was spun up for thirty years with a wind stress climatology derived from COADS (daSilva et al. 1995). The surface boundary conditions for temperature and salinity can be written as

$$\kappa_h(T, S)_z = (Q^T, Q^S).$$

The heat (Q^T) and virtual salt (Q^S) fluxes were computed from relaxation to a monthly sea surface temperature climatology derived from an 11-yr time series of AVHRR satellite measurements (Smith 1992; KR) and the monthly Levitus sea surface salinity climatology. Thus,

$$Q^T = \Delta z_1(T^* - T_1)/\tau_1,$$

$$Q^S = \Delta z_1(S^* - S_1)/\tau_2,$$

where Δz_1 is the thickness of the uppermost model level, $\tau_{1,2}$ is the damping timescale, and T^* and S^* are the reference temperature and salinity for the particular grid point determined by linear interpolation in time from the monthly climatology. Here, T_1 and S_1 are the prognostic temperature and salinity of the uppermost model level. The timescale for relaxation to the SST was set at 30 days and that for surface salinity was set at 120 days. The longer timescale for salinity yields realistic freshwater fluxes when diagnosed from the model integration (e.g., Tziperman et al. 1994). After the spinup, daily-averaged surface (10 m) wind stress from the European Centre for Medium-Range Weather Forecasts (ECMWF) wind analyses (ECMWF 1994) for the years 1985–95 was applied. The wind stress τ was computed using the standard bulk formula of Trenberth et al. (1989). The results below are derived from model fields averaged every five days.

3. Structure of the model OFZ

The averaged temperature and salinity from the model at 5 m are shown in Figs. 2a and 2b, respectively. The heavy dashed lines in each plot indicate the location of the maximum horizontal gradient in the subarctic and subtropical frontal zones. The SAFZ can be distinguished in both fields in the western part of the basin (near 42°N). Both isotherms and isohalines in the western SAFZ are more compact and farther north than in the Levitus climatology (not shown), indicating that the model's representation of the Kuroshio current is located too far to the north. The isotherms diverge across the central and eastern basin; the salinity gradient also diminishes but not as markedly. The STFZ is also apparent near 30°N, but is more diffuse than the SAFZ, especially in the temperature field. Consistent with observations, the STFZ is more apparent in salinity than in temperature.

A zonal average across the central Pacific from 180° to 170°W of the model temperature (Fig. 3a) and salinity (Fig. 3b) climatology for February shows the SAFZ to extend down several hundred meters with little meridional displacement. The salinity gradient weakens slightly with depth. The strong horizontal gradients in the SAFZ near 40°N are the juxtaposition of the model's Kuroshio Extension Front (KEF), the Kuroshio Bifurcation Front (KBF), and the Subarctic Front. The KEF is too far north because of the overshoot of the model's Kuroshio, but its gradients are weaker than the other two fronts, consistent with observations. The strong horizontal gradients with almost vertical isopleths of temperature and salinity over the upper 400 m are indicative of the KBF (e.g., Zhang and Hanawa 1993). The northernmost section of this strong frontal region, with salinity of 33.8 psu and lower, is indicative of the Subarctic Front.

The STFZ is much shallower than the SAFZ and is displaced southward with depth, consistent with climatological observations (e.g., White et al. 1978). Synoptic observations in the STFZ in the central-to-eastern Pacific (e.g., Roden 1980a) often show mixed layers as deep as 100 m and the southward displacement with depth is not as marked in synoptic fronts. Whereas the STFZ in the central-to-eastern Pacific is usually iden-

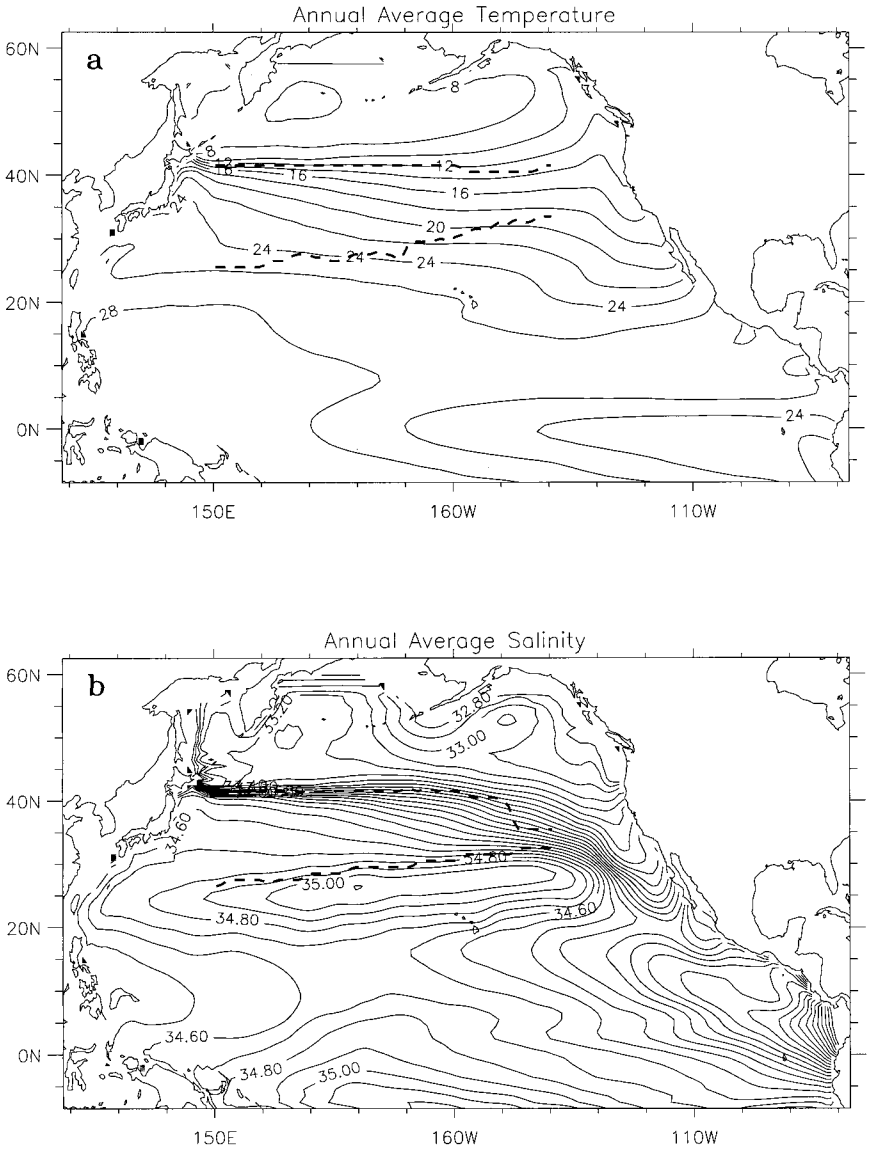

FIG. 2. Annual averaged temperature (°C) and salinity (psu) from the model at 5 m. The thick dashed lines represent the position of the model subarctic and subtropical fronts.

tified with the 18°C isotherm and the 34.8 psu isohaline, here the fronts are not coincident, and the strongest surface temperature gradient lies at about the the 22°C isotherm. The subsurface temperatures are too high as evidenced by the 18°C thermostad of subtropical mode water (STMW). In the central Pacific, STMW should have temperatures of about 16°C (e.g., White et al. 1978; Bingham 1992; Suga et al. 1997). The subtropical salinity gradient weakens and is displaced southward with depth. The intermediate salinity minimum is apparent at depth in the subtropics. There is very little seasonal change in subsurface structure. In August (not shown), the surface subtropical front in both temperature and salinity migrates northward. The maximum salinity gradient is located near 31°N; the maximum temperature gradient is no longer in the subtropical zone but appears to have migrated toward the SAFZ (see also Fig. 1).

The frontal zones are clearly delineated in maps of the magnitude of the horizontal temperature gradient. In the temperature climatology at 5 m for February (Fig. 4a), the OFZs show up as broad bands of high-temperature gradient. The SAFZ is a region of high-temperature gradient (>0.8°C/100 km) centered just north of 40°N and stretching zonally across most of the basin. The corresponding salinity front (not shown) is collocated with the temperature front but in a narrower band of high gradients (>1.35 psu/1000 km). The STFZ is the region of high (>0.6°C/100 km) temperature gradient that originates in the far western basin around 23°N and stretches eastward and slightly northward across the

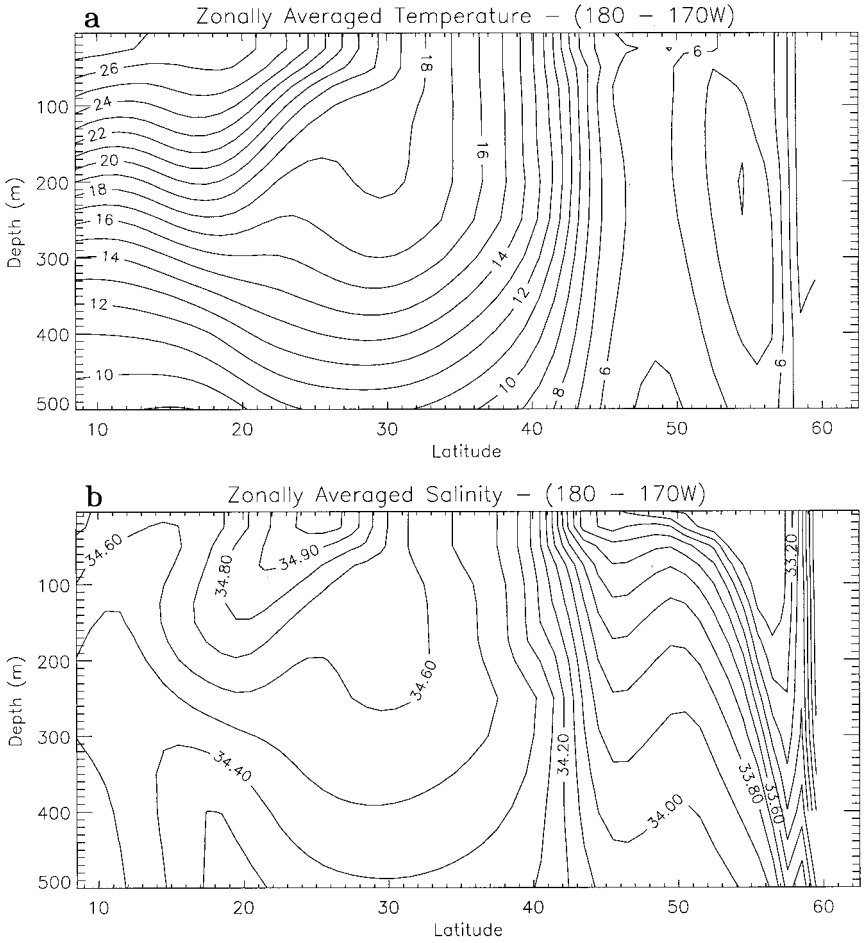

FIG. 3. Meridional sections of the February temperature (°C) and salinity (psu) climatologies from the model, averaged zonally over 180°–170°W.

basin. The gradient in August is shown in Fig. 4b. The subarctic temperature front is located in about the same place in August and February, but the strength changes with season as does the width of the frontal zone. For example, the peak gradient in the SAFZ in February at 180°E is 1.8°C/100 km; in August it is approximately 1.3°C/100 km. In contrast, the gradient in the eastern basin, from 170° to 145°W, is stronger in August than in February. Roden (1980b) found that along 165°E the peak gradients in the SAFZ occurred in winter. The AVHRR images of Fig. 1 indicate that this is true west of about 170°E. East of 170°E, the peak gradient in the AVHRR data is found during summer. The model subtropical temperature front is prominent in February but is not evident at the surface in August, consistent with observations (e.g., Roden 1975, 1980b; White et al. 1978; KR). It is not surprising that the SST gradient matches well with that from KR (see Fig. 1) since the model surface heat fluxes are derived from the same SST product used in their analysis. However, as will be shown later, the direct heat forcing is not the only important term in producing variations in the temperature gradient. At 100 m, the SAFZ is almost coincident with its surface expression and has similar strength (Fig. 4c). The STFZ temperature gradient at 100 m is slightly stronger and narrower, and is displaced slightly south of the annual mean surface front. Such a displacement and intensification of the STFZ temperature gradient with depth is consistent with observations in the western and central North Pacific (e.g., White et al. 1978). There is little seasonal variability in the subarctic and subtropical salinity fronts (not shown), although the salinity gradient in the central part of the SAFZ is stronger in August than in February.

The annual averaged horizontal density gradient at 5 m is shown in Fig. 4d. The contour increment chosen for the density gradient map is approximately equal to the change in density gradient that would result from the corresponding contour increment for the temperature gradient. The region of high surface density gradient just north of 40°N is primarily confined to west of 160°E, compared to the more eastward extent of high surface temperature or salinity gradients; that is, in the SAFZ the horizontal temperature and salinity gradients tend

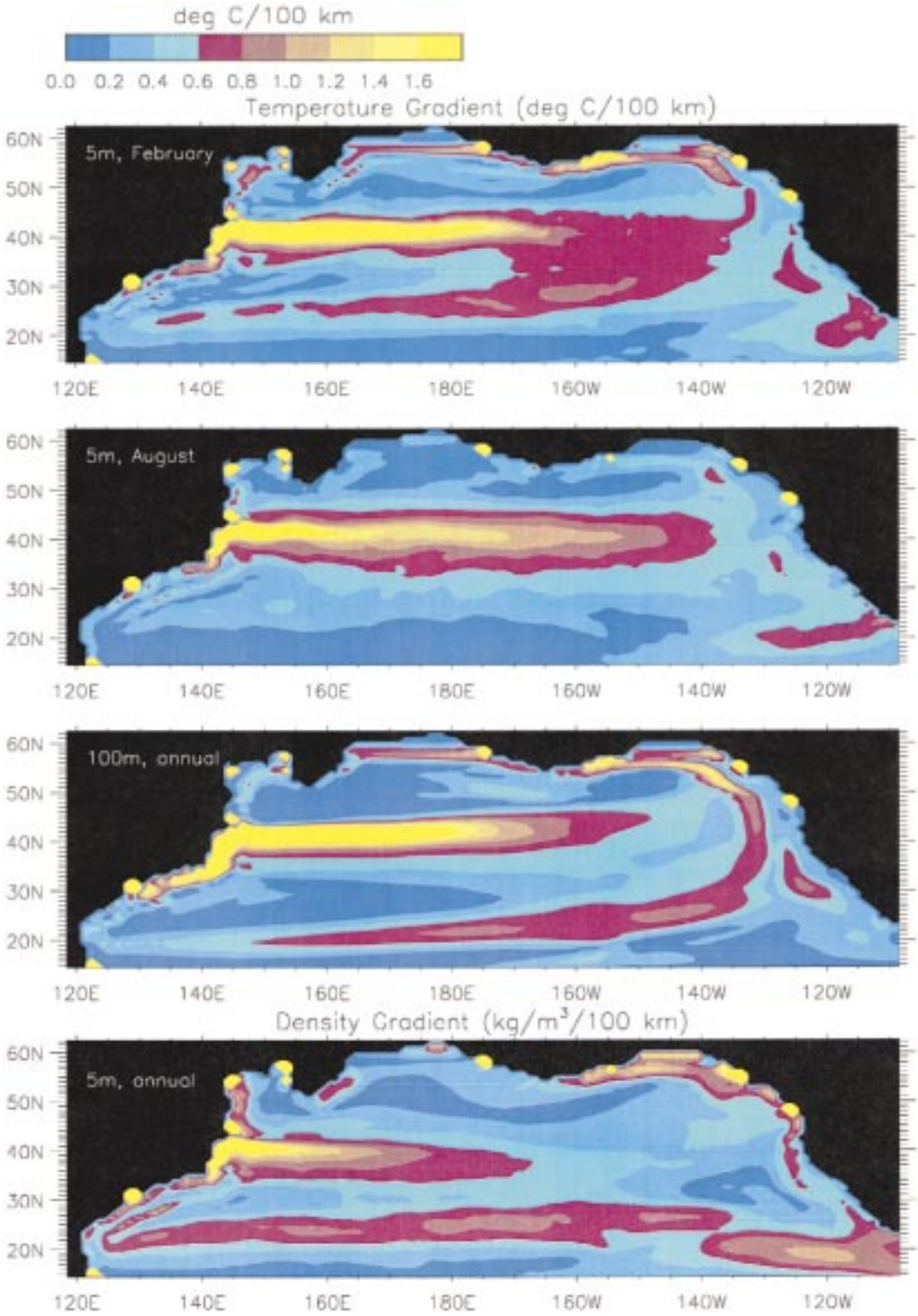

FIG. 4. Magnitude of the model's horizontal gradient of (a) temperature climatology for February at 5 m, (b) temperature climatology for August at 5 m, (c) annual averaged temperature at 100 m, and (d) annual averaged density computed from the monthly temperature and salinity climatologies at 5 m. Note that the contour levels for the density plot are at every 0.04 kg m^{-3}/100 km.

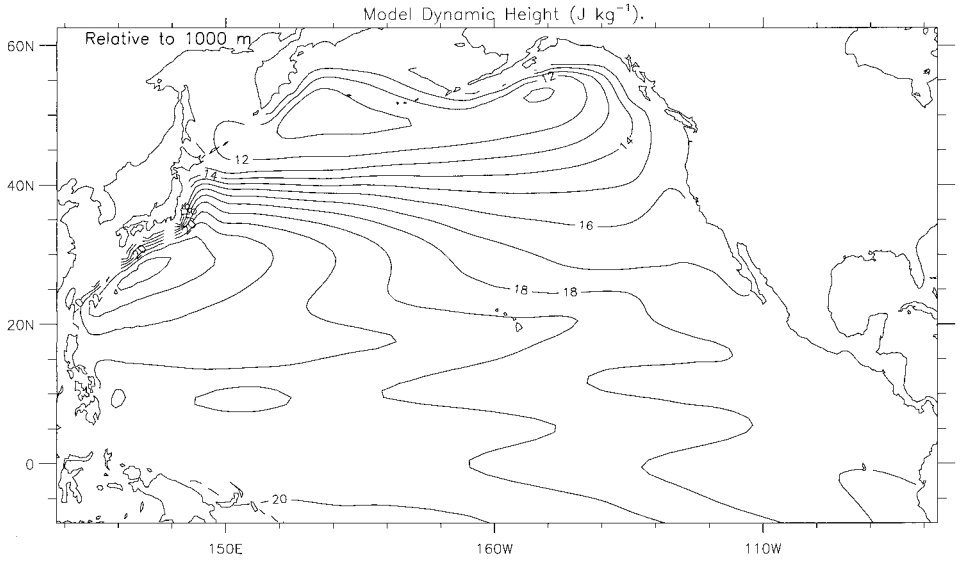

FIG. 5. Annual averaged model dynamic height (J kg^{-1}) with respect to 1000 m computed from the monthly temperature and salinity climatologies.

to be density compensating. Yuan and Talley (1996) show that during summer there is very little density compensation in the SAFZ in the western Pacific. This region of high density gradient in the model is associated with the confluence of the salty Kuroshio Extension current and the fresh Oyashio current. In the model, the Kuroshio overshoots its observed separation latitude of about 35°N. Although it returns slightly southward after leaving the coast, the strongest gradient in dynamic height (Fig. 5) at 160°E is in the region of the North Pacific Current, that is, about 40°N, rather than in the Kuroshio Extension. This frontal zone is identifiable as the SAFZ by the 33.8 psu isohaline, which is embedded within the region of the strongest temperature and salinity gradients in the model and is often used observationally as the southern limit of the SAFZ (e.g., Lynn 1986; Roden 1991). In the central North Pacific, away from the strongest influence of the model's Kuroshio Extension, the SAFZ density gradient is relatively weak compared to the temperature and salinity gradients. A moderately strong ($>$0.12 kg m^{-3}/100 km) subtropical density gradient starts at 23°N in the west and extends eastward across the entire basin. In the STFZ, the annual averaged temperature and salinity fronts are not density compensating.

Direct meteorological forcing of fronts is generally limited to the depth of the high stability layer underlying the surface (Roden 1980a). The boundaries of the SAFZ are often defined by the outcrop of the isohalines of the permanent halocline in the subarctic ocean. This halocline results in a hydrostatic stability maximum in the subarctic ocean that is located at about 150 m in winter. During winter and early spring, a shallow seasonal thermocline develops south of about 37°N, which leads to a hydrostatic stability maximum at about 50 m (Roden 1991). Until the seasonal warming has progressed far enough northward to create a seasonal thermocline up to the latitude of the SAFZ, there exists what Roden (1991) refers to as a seasonal ''low stability gap.'' This gap is where, in winter and early spring, there is a lateral minimum in the high vertical stability layer between 37° and 43°N. This feature is key to the formation of North Pacific central mode water (NPCMW) in this region (e.g., Suga et al. 1997). The hydrostatic stability can be expressed in terms of the Brunt–Väisälä frequency N:

$$N^2 = -g\left(\frac{1}{\rho}\frac{\partial \rho}{\partial z} + \frac{g}{c^2}\right),$$

where g is the acceleration due to gravity and c is the speed of sound. The model Brunt–Väisälä frequency as a function of depth and latitude in midbasin is shown in Fig. 6. For February, low values of N^2 penetrate from the surface to close to 200 m from north of 30°N to about 43°N. The temperature and salinity structure in this region is more likely to be influenced by convection forced from surface heat and freshwater fluxes. The region of low stability in the model extends farther south than in the observations, including the North Pacific subtropical mode water formation region as well as that of NPCMW. In the model (Fig. 6b) and in observations (Roden 1991), the low-stability region narrows during spring until it disappears in summer/early fall. The midlatitudes are then covered by a shallow high stability region (due to solar heating) that limits the possible influence of convection.

In summary, the model appears to simulate the location of the frontal zones reasonably well. The gradients are generally consistent with observations. The western SAFZ in the model is a combination of a true

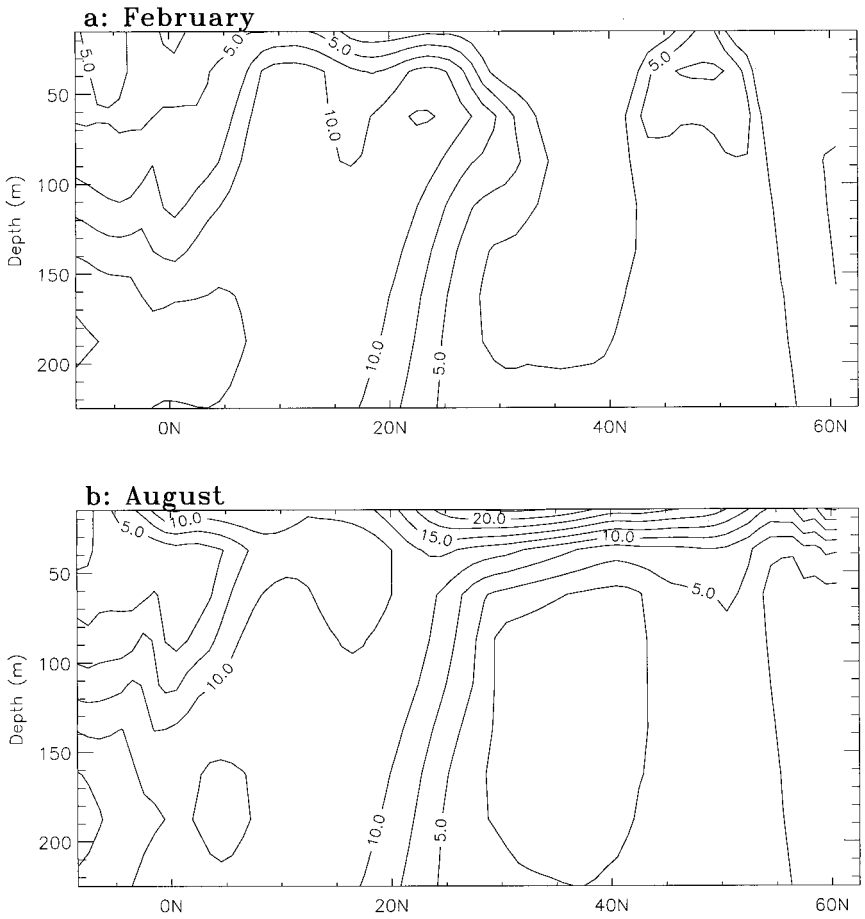

FIG. 6. Model Brunt–Väisälä frequency computed from the (a) February and (b) August temperature and salinity climatologies, averaged zonally over 180°–170°W.

SAFZ and a mixture of the Kuroshio and Oyashio Extensions due to the overshoot of the Kuroshio Extension and its influence on the west wind drift current. The model produces a seasonal variation in the vertical hydrostatic stability consistent with observations. However, the region of the low stability gap covers a larger area than found in the observations.

4. Seasonal meridional frontogenesis and frontolysis

Since the OFZs are primarily zonally oriented, this section focuses on the seasonal cycle of meridional frontogenesis. The meridional derivative of the monthly averaged zonal wind stress for February and August is shown in Fig. 7a. The February plot clearly shows an area ($\partial\tau_x/\partial y >$ zero) of meridional Ekman convergence roughly coincident with the STFZ. In the region of the SAFZ, the meridional divergence is weak in February, and the convergence is very weak in August. The monthly averaged heat flux into the ocean for February and August, inferred diagnostically, is shown in Fig. 7b. The heat fluxes are in agreement with climatology in their large-scale patterns and amplitude. Very strong meridional frontolysis due to heat forcing would be expected in February in the western and central portions of the SAFZ where $\partial Q/\partial y > 0$ (less cooling in the colder water north of the front). Meridional frontogenesis would be expected in the western and central portions of the STFZ. The heat flux pattern in August shows that there should be a broad region of frontolysis due to heat forcing across much of the subarctic–subtropical transition zone during this month. The February and August averages of the evaporation minus precipitation ($E - P$), inferred diagnostically, are shown in Fig. 7c. The general patterns of $E - P$ also seem to be in agreement with climatology (e.g., see, Qiu 1995), except for the structure in the region of the model's Kuroshio Extension. One can infer from these figures that there should be meridional frontolysis due to freshwater flux in the western and central portions of the SAFZ in both seasons [$\partial(E - P)/\partial y > 0$, that is, larger salinity increase in the fresher water north of the front].

The meridional frontogenetic balance for temperature was computed from 5-day averaged fields according to

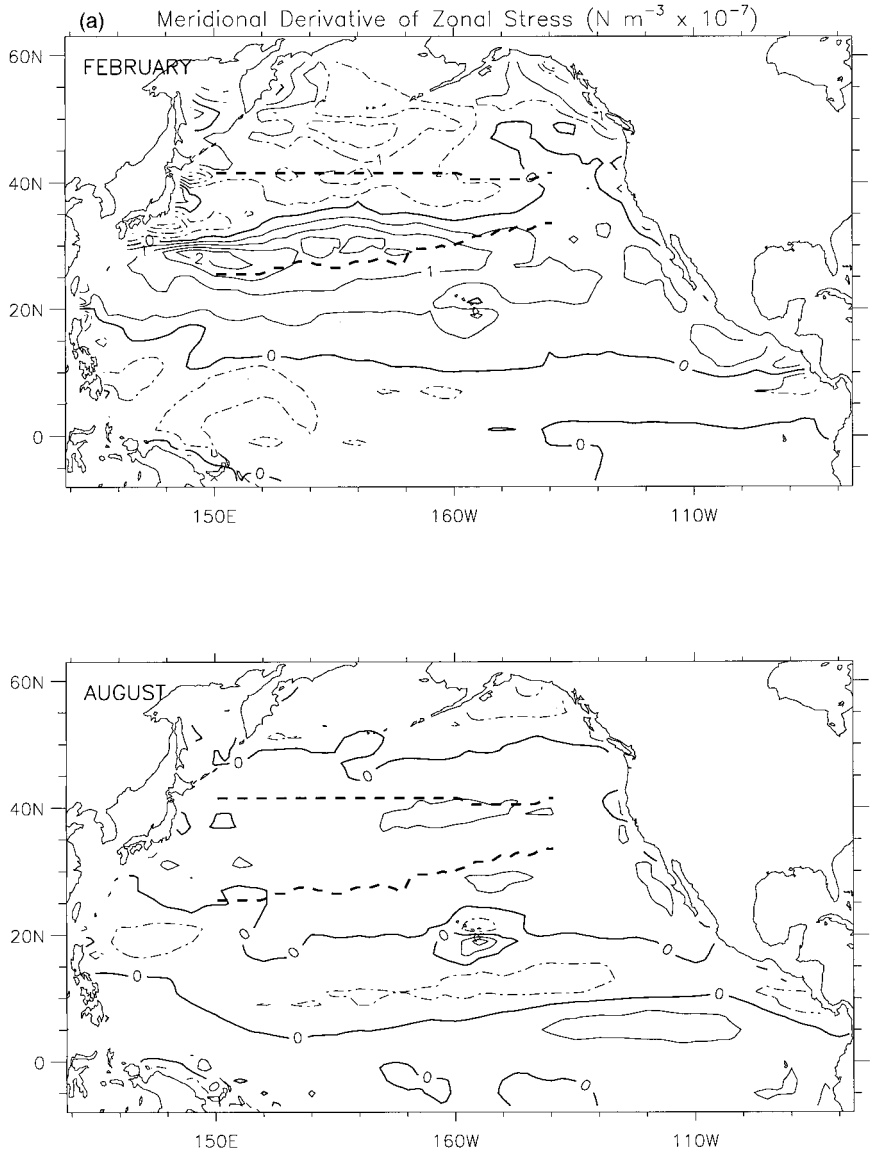

FIG. 7a. Meridional derivative of the climatological zonal wind stress for February and August. Units are 10^{-7} N m^{-3}. The thick dashed lines are the same as for Fig. 2a and represent the position of the model subarctic and subtropical temperature fronts.

$$\frac{\partial}{\partial t}\left(\frac{\partial T}{\partial y}\right) = \frac{\partial}{\partial y}\left(u\frac{\partial T}{\partial x}\right) + \frac{\partial}{\partial y}\left(v\frac{\partial T}{\partial y}\right) + \frac{\partial}{\partial y}\left(w\frac{\partial T}{\partial z}\right) + \frac{\partial}{\partial y}[A_h(\nabla^2 T)] + \frac{\partial}{\partial y}\left[\kappa_h\left(\frac{\partial^2 T}{\partial z^2}\right)\right] + R,$$

where T, u, v, w represent 5-day averaged quantities and R represents the residual balance (contributions from the nonlinear terms due to coherent variations on timescales shorter than five days as well as the impact of convective adjustment). The meridional frontogenetic balance for salinity (S) was computed in a similar manner. The first term on the right-hand side of the equation is the shearing term and is due to the differential zonal advection of heat (or salt). The second term is the convergence term and is due to the differential meridional advection of heat. The next term is the tilting term and is due to the differential vertical advection of heat. The fourth term is the differential horizontal diffusion term. The fifth term is the differential vertical diffusion term which at the surface includes the surface heat or freshwater flux. To remove some of the small-scale variations in the balance, which are not of interest for the seasonal cycle, the balance is computed over a zonal band. The seasonal cycle presented below is calculated as monthly averages from the 11-yr integration.

The direct heat flux and freshwater flux forcing is represented in the model as a boundary condition (at

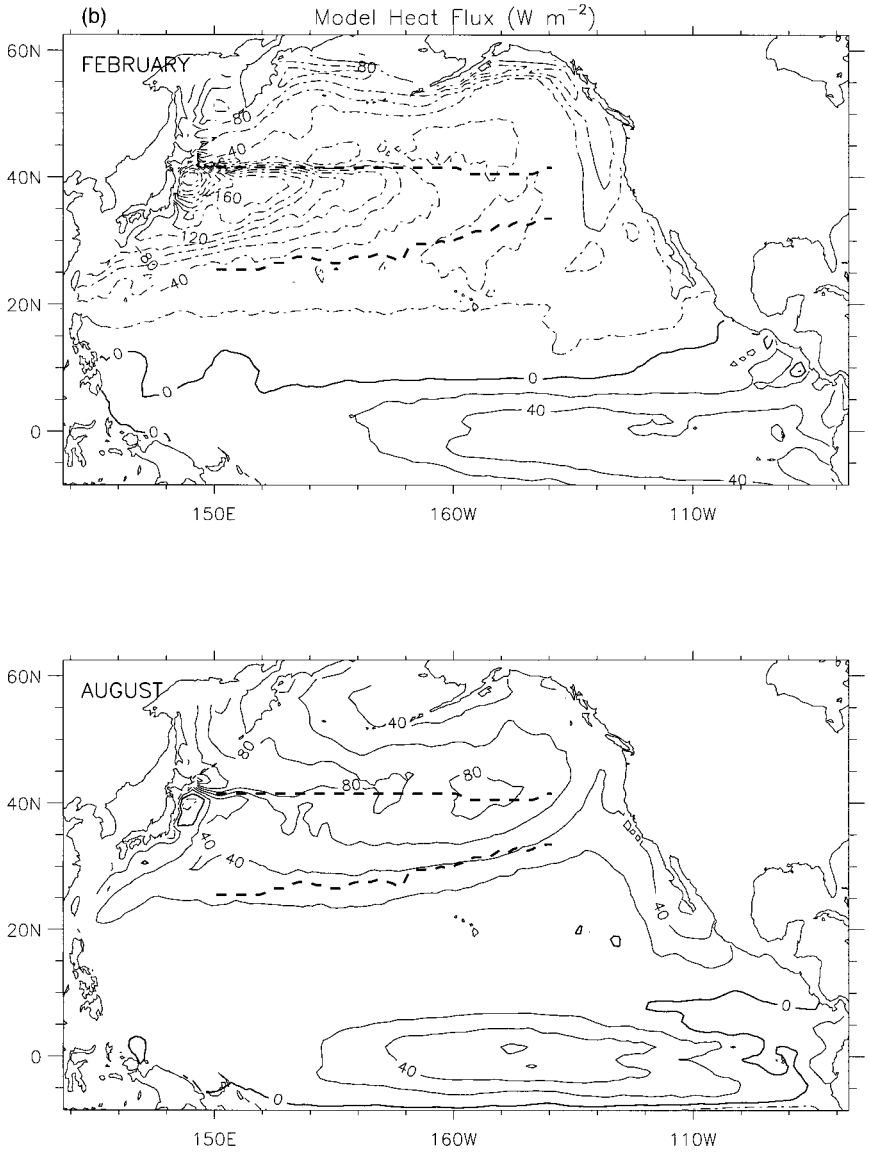

FIG. 7b. Climatology of the model-inferred heat flux (W m^{-2}) into (positive numbers) the ocean for February and August. The thick dashed lines are the same as for Fig. 7a.

the top model level) in the vertical diffusion term (see section 2). Since the interior vertical diffusion is normally very small, the differential diffusion term at the top model level will mostly represent the differential heat flux or freshwater flux forcing. The differential horizontal diffusion term was always very small and is therefore not displayed here. Balances using model output at every timestep determined the dominant contribution to R. These calculations showed the overwhelming contribution to the total was due to the convective adjustment (which is implemented in the model as vertical mixing to remove any density inversions within a single timestep). Therefore, the R term can be thought of in terms of a mixing term dominated by convection. This term is very important, especially in reducing the effects of differential cooling.

For the differential meridional advection, the Ekman convergence is calculated directly to compare with the convergence in the model's surface velocity. Since, in the model, the surface forcing is applied as a body force over the upper layer, the Ekman convergence is computed from the associated Ekman meridional velocity: $V_e = -\tau_x/\rho f h$, where τ_x is the zonal wind stress component and h is the depth of the model's surface layer (15 m). In the following subsections, the seasonal cycle of frontogenesis is investigated in the western (160°–170°E), central (180°–170°W), and eastern (160°–150°W) portions of the OFZs.

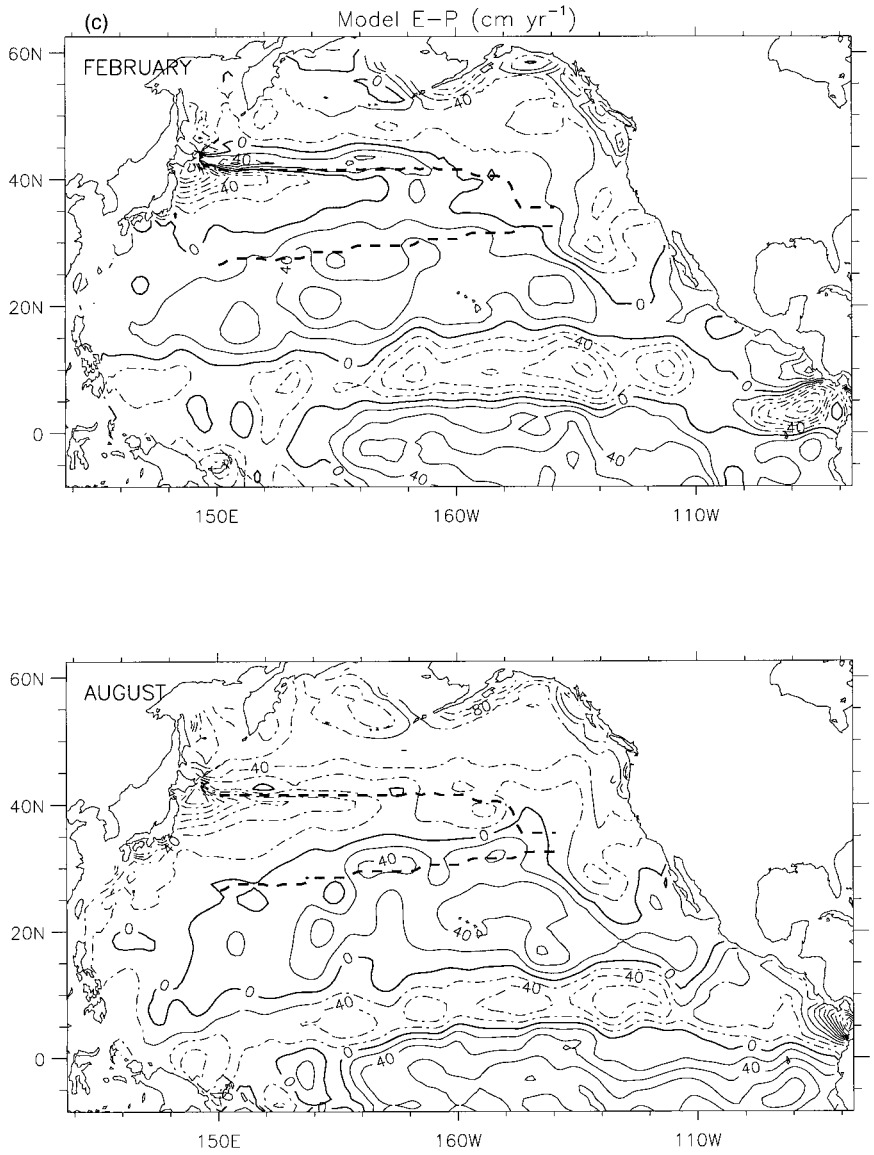

FIG. 7c. Climatology of the model-inferred evaporation minus precipitation (negative freshwater flux in cm yr^{-1}) for February and August. The thick dashed lines are the same as for Fig. 2b and represent the position of the model subarctic and subtropical salinity fronts.

a. Temperature

The seasonal cycle of temperature frontogenesis, the dominant terms in the frontogenetic balance, and the temperature gradient at the surface in the western Pacific (160°–170°E) are shown in Fig. 8a. Since the temperature gradient is almost always negative, negative values (solid contours and shaded regions) represent frontogenetic processes while positive values (dashed contours) represent frontolytic processes. The thick dashed lines in the frontogenesis plot show the location of maximum meridional temperature gradient between 36.5° and 45.5°N for the SAFZ and between 22.5° and 34.5°N for the STFZ.

The subarctic temperature front exhibits a strong seasonal cycle, with a maximum of 3.0°C/100 km in winter and a minimum of 1.4°C/100 km in summer/fall, but little seasonal migration of the position of the maximum gradient. The SAFZ of the Levitus climatology does not vary much in strength or position and is significantly weaker (by up to 50%) than the model during winter and spring (e.g., see Yuan and Talley 1996). The subtropical temperature front is strongest (>0.6°C/100 km) in the spring and the location of the maximum surface gradient migrates substantially over the year. The frontogenesis plot shows the STFZ migrating northward during spring, undergoing frontolysis during summer and

then moving southward during winter. For this region, the total flow convergence term (not shown) and the Ekman convergence term match very well indicating that most of the convergence of meridional advection is wind driven and, as expected, the flow is primarily geostrophic alongfront. The vertical diffusion term (primarily due to surface heating) is extremely strong relative to the frontogenesis and through much of the year is frontolytic in the SAFZ and frontogenetic in the STFZ (as shown in Fig. 7b). However, the residual (which was shown to be mostly due to convective mixing) is also extremely strong relative to the frontogenesis and acts against the vertical diffusion gradient and the Ekman convergence much of the year. The residual term is large during winter and spring, consistent with the low vertical stability in the top layer. The sum of the vertical diffusion term and the residual term, also shown, represents the heating (or cooling) of the surface layer due to surface heat flux and vertical mixing. The convection effectively extends the influence of the surface cooling below the upper layer of the model. Convection can also occur in response to advective effects at the surface and, in fact, the convective term here is primarily a response to the Ekman convergence in the SAFZ in late winter and early spring. It is only partially due to surface cooling in the northern part of the SAFZ during late winter. In the SAFZ, the sum of the vertical diffusion term and residual term is at least as important as the Ekman convergence and it provides a balance to the Ekman convergence and dominates that term in late fall/early winter. The sum of the Ekman convergence, the vertical diffusion gradient and the residual terms is shown in the bottom left-hand panel. Compared with this balance, the shearing term provides a significant contribution to SAFZ frontogenesis and midlatitude frontolysis during fall and winter. Surface heat flux and convective effects dominate in late spring and summer over most of the domain.

At 100 m, the subarctic temperature gradient (Fig. 8b) is comparable in intensity to that at 5 m, but the maximum gradient (3.4°C/100 km) occurs slightly earlier, in December. The front is collocated with that at 5 m. In contrast, Yuan and Talley (1996) show the subsurface front to be displaced a few degrees north of the surface front. The subtropical temperature front shows little seasonal migration and is located several degrees south of the surface front. Almost all the frontogenesis in the SAFZ is due to the shearing term while almost all the frontolysis is due to the residual (mostly differential convection) term. The effect of differential convection is opposite in sign to that at the surface. The meridional band where the residual term is important in February is smaller at this depth than at the surface, which corresponds to the shrinking (with depth) of the zone of low vertical stability (Fig. 6a). There is very little frontogenetic activity in the STFZ.

The subarctic surface temperature front in the central North Pacific (180°–170°W, Fig. 9) exhibits a small seasonal variation in strength and in position. The front is at its maximum strength (1.4°C/100 km) during spring while at its northernmost position. It is weakest (1.1°C/100 km) and farthest south during winter. The frontogenesis/frontolysis in the central Pacific results from the balance between the Ekman convergence and the net heat flux forcing (i.e., heat flux and vertical convection) with Ekman convergence dominating the STFZ frontogenesis during fall and the vertical mixing and heating dominating the STFZ frontolysis during summer. The shearing term is small but is of some significance to the frontogenesis of the SAFZ during winter and early spring when compared to the balance of the dominating terms. As for the western basin, the vertical convection term in the SAFZ during winter is primarily a response to the effect of Ekman convergence, with some response to the frontolytic nature of the surface cooling. It is this convective term and the shearing term which lead to the frontogenesis in the northern part of the SAFZ during winter. The surface heat flux is responsible for the frontolysis in the SAFZ during late spring/early summer.

The seasonal cycle of the model frontogenesis in the central North Pacific differs from the observed temperature frontogenesis from AVHRR data in the SAFZ (KR). There is a clear tendency for frontolysis in June and frontogenesis in January at the model front (location of maximum gradient) and northward in the SAFZ. More importantly, the phase of the maximum gradient differs from observations, with the maximum gradient in March/April in the simulation and in July in the AVHRR data (and other climatologies) in this region. One would expect the temperature fronts in the model in the central North Pacific to be similar to the fronts in KR in areas where differential heat flux forcing is the dominant term in the frontogenesis since the same data is used for the model's heat flux estimation. The difference in the seasonal cycle shows that other factors must be important in the model. This will be discussed in more detail in section 5. The variability at 40°N (the location of the maximum gradient in fall), with a distinct annual cycle and a minimum gradient in spring, is in better agreement with the observations than the variability following the maximum gradient. Here, the frontogenesis signal is weak and is generally of opposite sign to that in the northern SAFZ with frontogenesis in June and frontolysis during winter.

At 100 m (not shown) almost all the frontogenesis/frontolysis in winter and early spring is explained by the residual term (convective overturning). The horizontal shearing term is frontogenetic in the SAFZ all year; it is the dominant term and achieves maximum frontogenesis in November–December.

In the eastern North Pacific (160°–150°W), the subarctic front is barely discernible as a separate front and has a small seasonal variation in intensity (Fig. 10). A separate subtropical front is discernible at the surface only in spring. In this eastern band, the seasonal cycle of the temperature gradient is in better agreement with

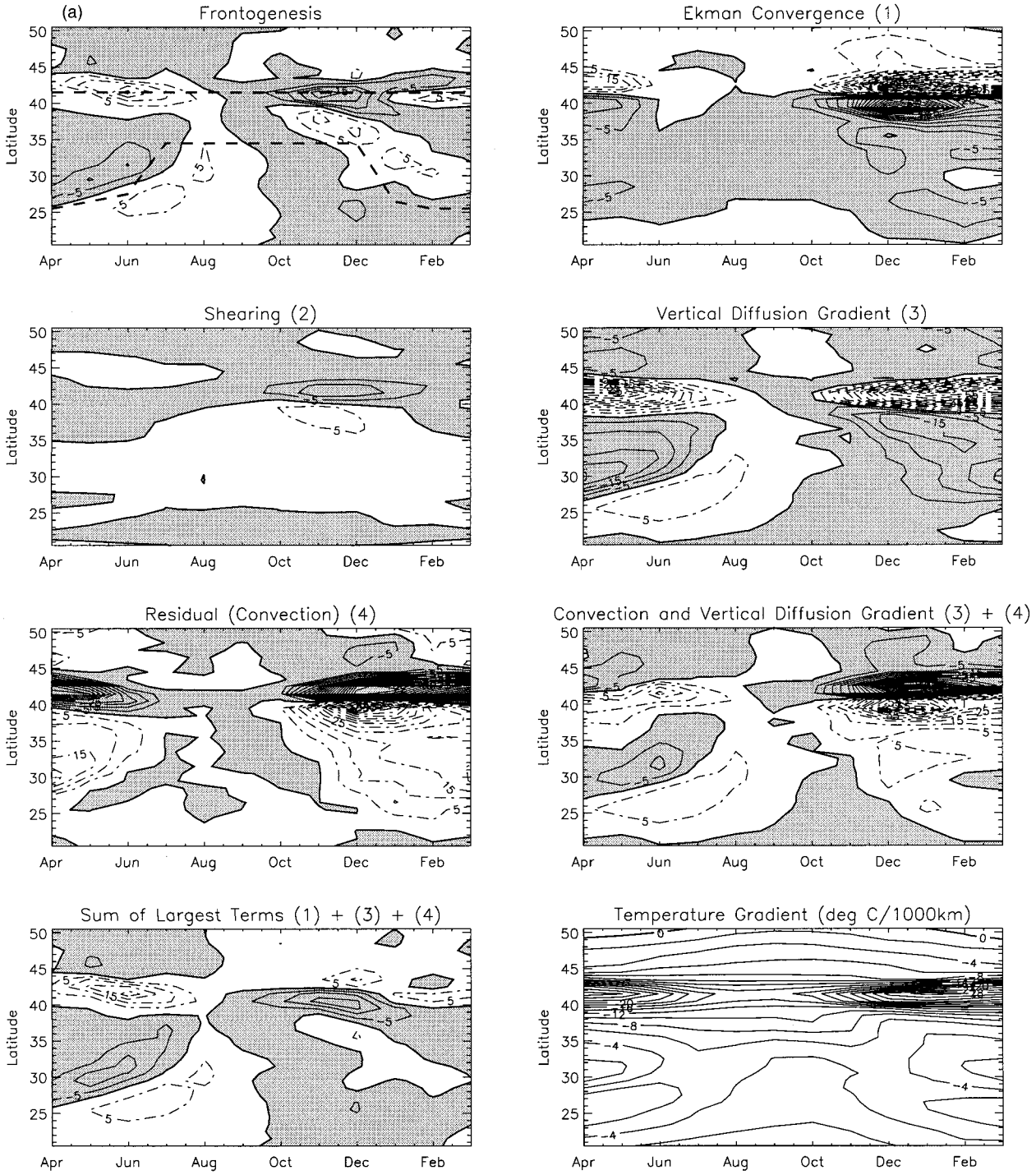

FIG. 8a. Meridional temperature frontogenesis at 5 m zonally averaged over 160°–170°E. For the frontogenesis panel (upper left) note that since the meridional temperature gradient is almost always negative, negative values (solid contours: shaded) represent frontogenesis. The thick dashed lines represent the position of the maximum gradient in the model SAFZ and STFZ. Also shown are the dominant terms, or their sums, contributing to meridional temperature frontogenesis. The units for the temperature frontogenesis panels are 10^{-5}°C km^{-1} day^{-1}. The contour interval is 5.0. The bottom right panel is the meridional temperature gradient in units of °C/1000 km. The contour interval is 2. See text for details.

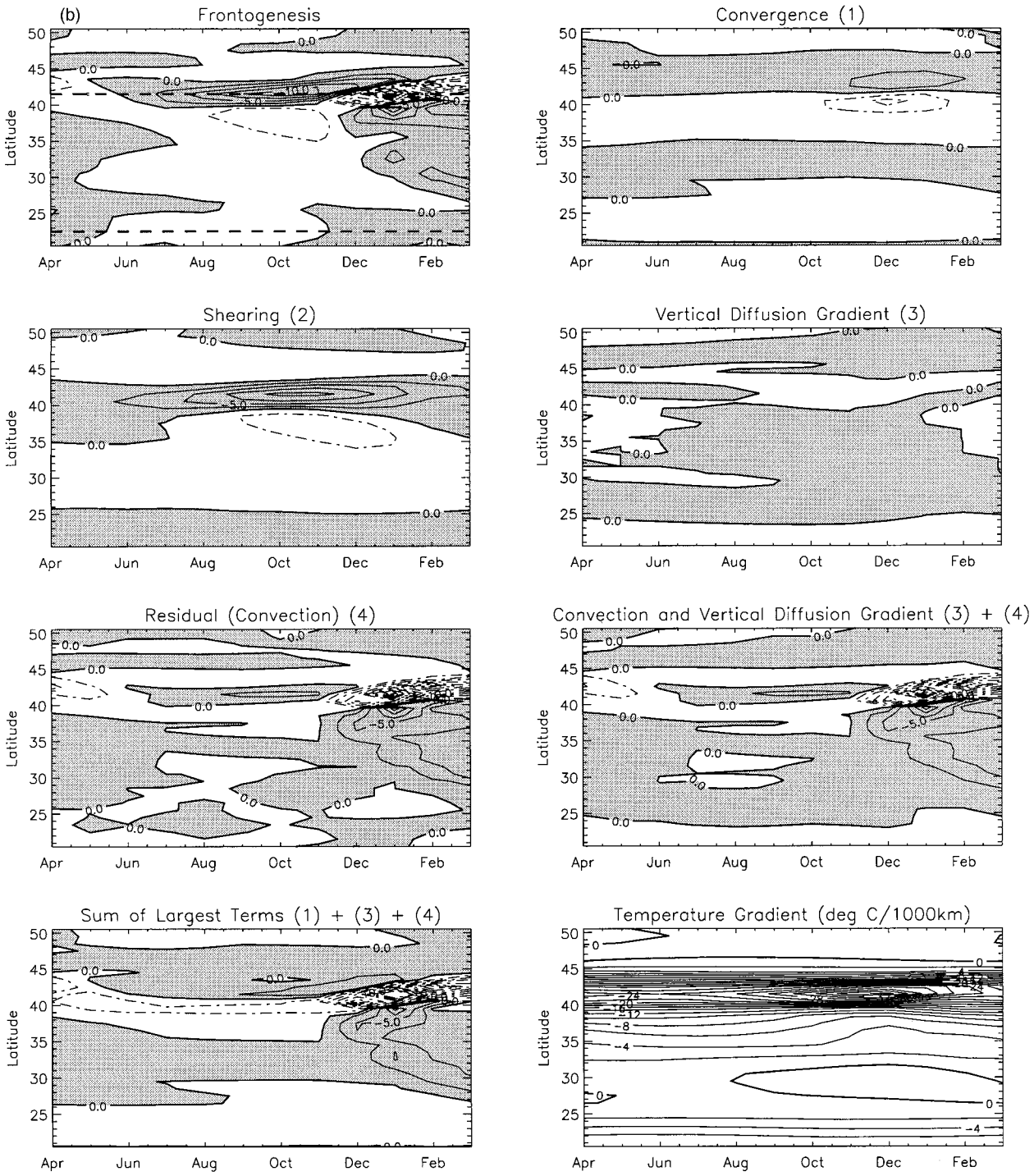

FIG. 8b. As for Fig. 8a but for 160°–170°E at 100 m and with a contour interval of 2.5 for the frontogenesis panels.

observations than in the central Pacific. The frontogenesis/frontolysis in the SAFZ is due primarily to the surface heat flux (frontolytic) and the differential vertical convection that is responsible for the frontogenesis during late winter/spring. The surface Ekman convergence, although active, primarily moderates the influence of the other processes. The Ekman convergence is frontogenetic for the SAFZ during summer/fall consistent with the findings of Yuan (1994) in the eastern Pacific. The shearing term is not significant to the meridional frontogenesis in the eastern basin. In the STFZ, most of the frontogenesis is due to the Ekman convergence

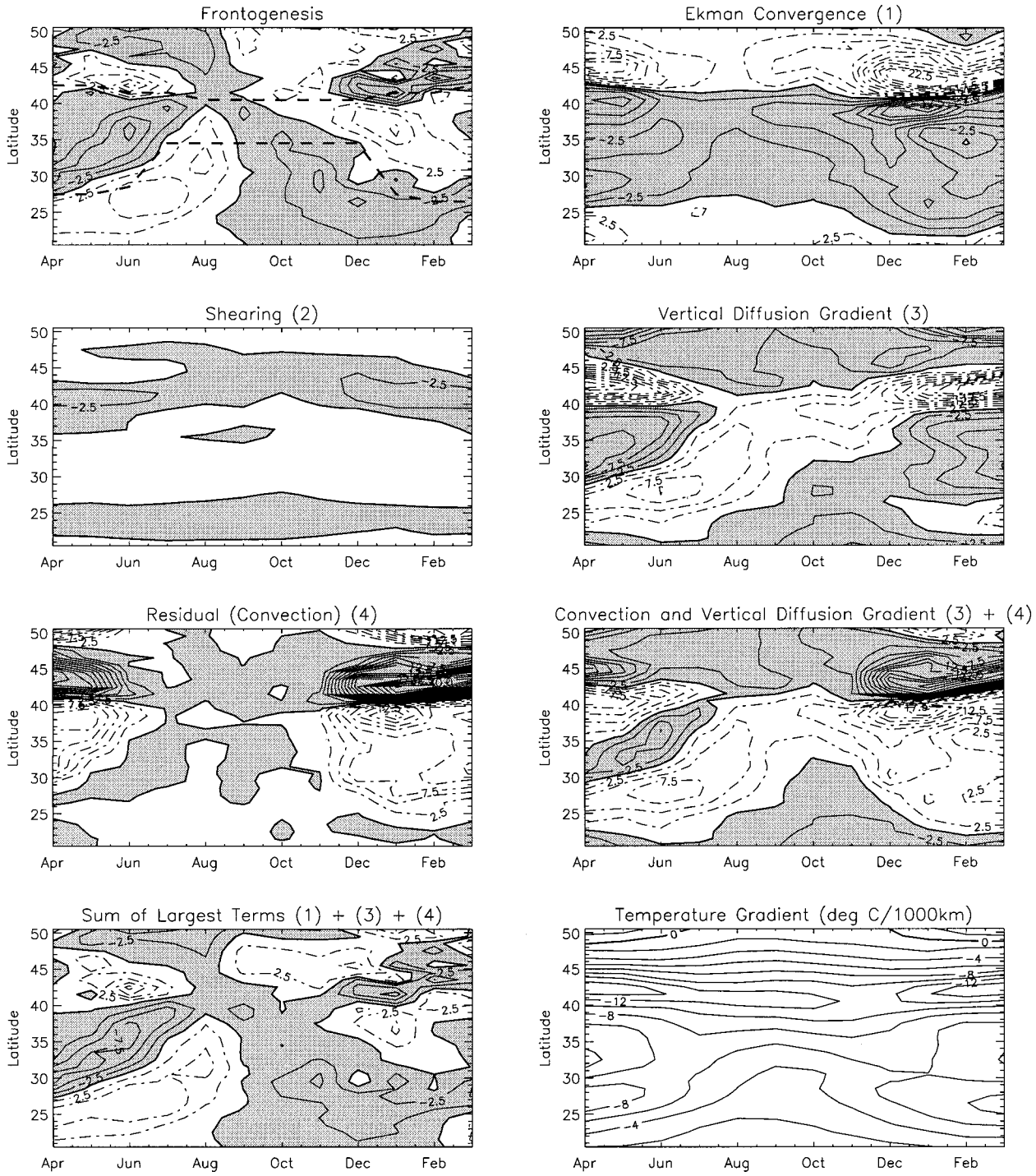

FIG. 9. As for Fig. 8a but for 180°–170°W at 5 m and with a contour interval of 2.5 for the frontogenesis panels.

term (see Fig. 7a) and most of the frontolysis is due to the net heat flux forcing, with the Ekman component dominating during winter and surface heating dominating during summer. At 100 m (not shown) there is very little frontogenesis/frontolysis and the OFZs stay relatively constant.

b. Salinity

For the analysis of salinity frontogenesis, each term is computed in the same manner as the terms in the temperature frontogenesis figures. The balance of dominant terms for salinity is given by the sum of the Ekman

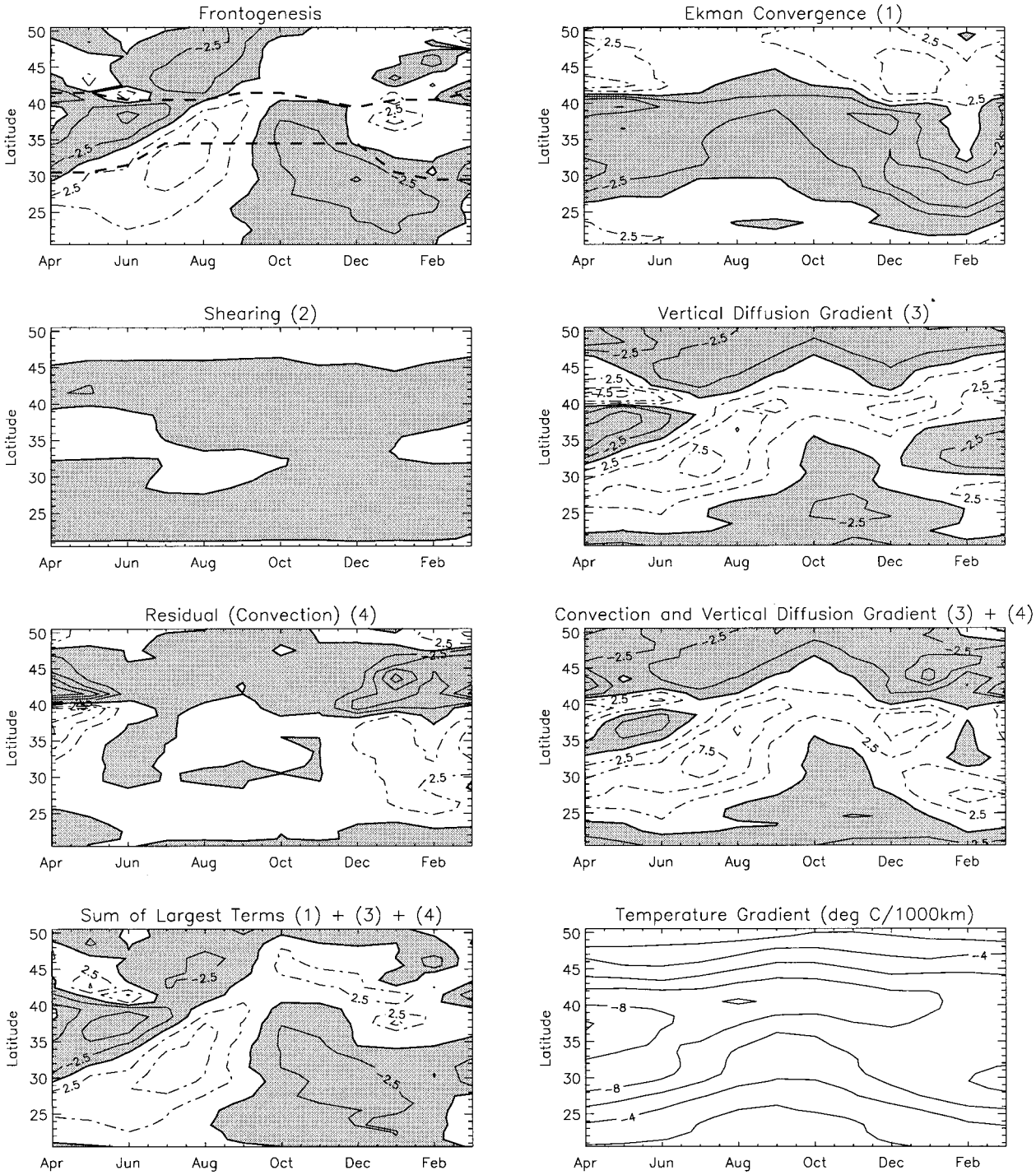

FIG. 10. As for Fig. 8a but for 160°–150°W at 5 m and with a contour interval of 2.5 for the frontogenesis panels.

convergence and the residual terms. Where the salinity gradient is negative (most of the figure), negative values in the plots (solid contours and shaded regions) represent frontogenetic processes and positive values (dashed contours) represent frontolytic processes.

The subarctic salinity front in the western North Pacific exhibits a strong seasonal cycle with a maximum of 0.4 psu/100 km in winter and a minimum of 0.3 psu/100 km in fall (Fig. 11). The position changes only about 1°. In the Levitus climatology the subarctic front has a maximum gradient of 0.2 psu/100 km in winter and spring. There is less seasonal variability in the subtrop-

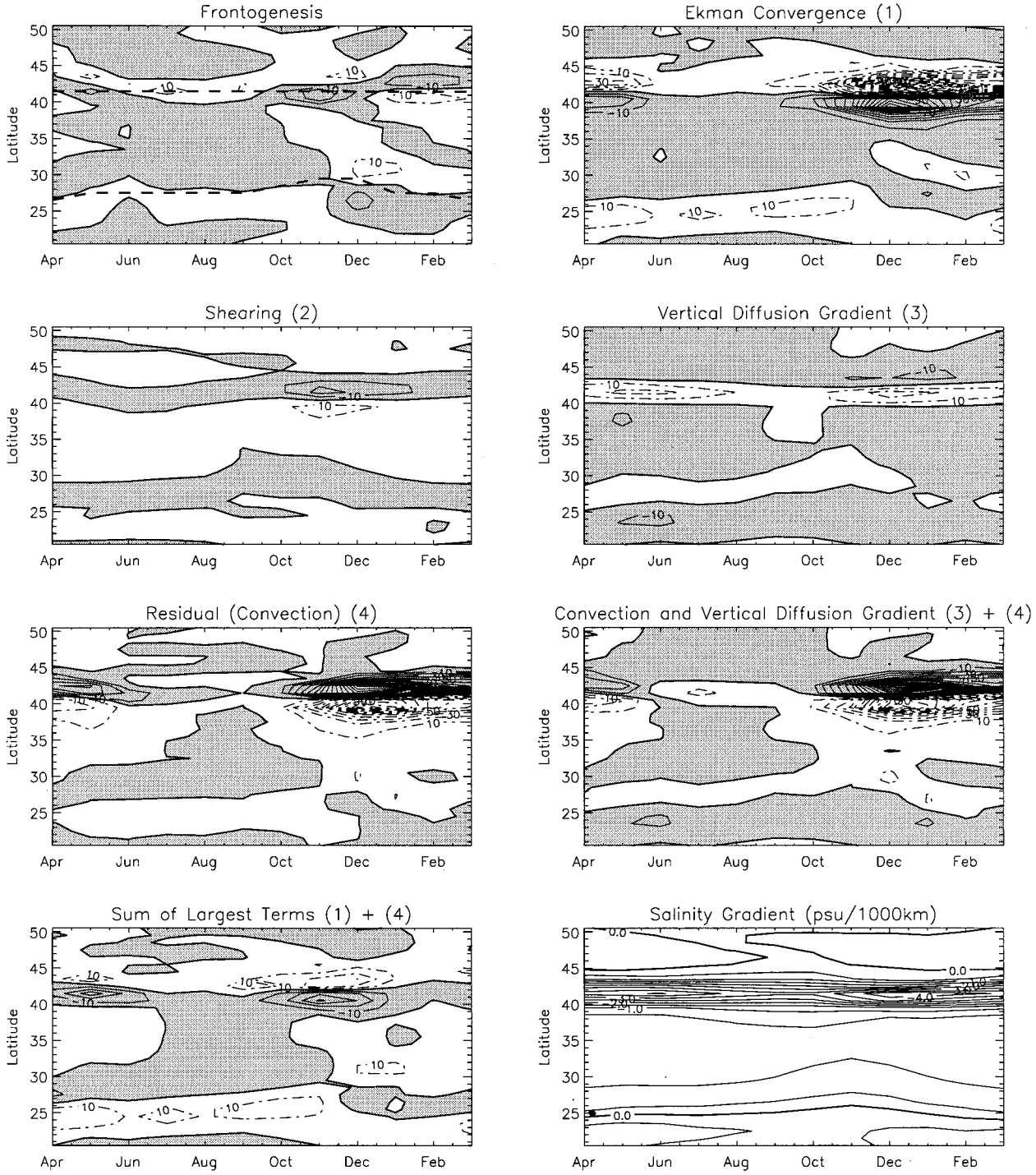

FIG. 11. Meridional salinity frontogenesis at 5 m for 160°–170°E. For the frontogenesis panel (upper left) note that since the meridional salinity gradient is usually negative (although not always, especially at the southern edge of the panel), negative values (solid contours: shaded) usually represent frontogenesis. The thick dashed lines represent the position of the model SAFZ and STFZ. Also shown are the dominant terms, or their sums, contributing to meridional salinity frontogenesis. The units for the salinity frontogenesis panels are 10^{-6} psu km^{-1} day^{-1}. The contour interval is 10.0. The bottom right panel is the meridional salinity gradient in units of psu/1000 km. The contour interval is 0.5. See text for details.

ical salinity front. The shearing term contributes to the SAFZ frontogenesis during fall and winter and is significant when compared to the dominant term balance. Differential freshwater flux is the primary contribution to SAFZ frontolysis during summer. The differential freshwater flux is strongly frontolytic throughout the year in the SAFZ and slightly frontolytic in the STFZ. In early summer, SAFZ frontolysis is associated with differential surface fluxes for both temperature and salinity, the maximum occurring in June for temperature and July for salinity. In addition, there is salinity frontogenesis at or just to the south of the front, with a maximum in May, primarily due to differential vertical convection. The residual (mostly due to convective mixing) is primarily in response to the Ekman convergence and differential heat flux rather than freshwater flux, at least between 35° and 45°N (compare with Fig. 8a). The sum of the vertical diffusion term and the residual term is shown in the third panel down on the right side. For the salinity frontogenesis, this term represents changes in surface layer salinity due to freshwater flux plus convective mixing. It is comparable to, but opposes the flow convergence term in the SAFZ. There is very little frontogenetic activity in the STFZ. At 100 m, the salinity frontogenesis variability and the causal mechanisms are very similar to those found for temperature and are not shown.

The subarctic salinity front in the central North Pacific also exhibits a seasonal cycle in strength and position (Fig. 12). The front is at its maximum strength in spring and summer (2.1 psu/1000 km) and is weakest in winter (1.6 psu/1000 km). The subtropical salinity front in the central North Pacific maintains a relatively constant strength, but shifts meridionally by about 3°. The seasonal migration of the salinity front is in good agreement with the observations. During summer and fall, the SAFZ undergoes frontolysis north of the front and frontogenesis south of the front so that the front migrates slightly southward. This reverses during winter. The frontogenesis pattern during summer and fall is due primarily to Ekman convergence. The frontogenesis pattern during winter/spring is primarily due to the vertical convection, enhanced by the shearing term especially in late spring. The freshwater flux in this region is frontolytic throughout the year in the SAFZ and the vertical convection is in response to the Ekman convergence and surface cooling. The patterns of frontogenesis and frontolysis in the SAFZ are coincident with those for temperature except for the periods of frontogenesis on the southern side of the salinity front from May to November. This frontogenesis is due to the stronger influence of meridional Ekman convergence on the salinity frontogenesis during this period and the lesser frontolytic influence of differential surface freshwater flux. In the STFZ, the Ekman convergence term dominates, enhanced by surface freshwater flux in summer and vertical overturning in winter. At 100 m (not shown), all the frontogenesis/frontolysis (except for a small amount of frontogenesis during fall and early winter in the SAFZ due to shearing) is explained by the residual term and appears very similar to the pattern of frontogenesis/frontolysis of the temperature at this location and depth. The ratio of the contour interval for Fig. 12 to that of Fig. 9 is approximately equal to the ratio of the thermal expansion coefficient to the expansion coefficient for salinity. Thus the high correlation between the frontogenesis patterns for temperature and salinity in the SAFZ helps to explain how the density compensation is maintained in the model front.

In the eastern Pacific the patterns and frontogenetic balance are very similar to those in the central Pacific, except the terms are weaker.

5. Discussion

This study confirms previous observational analyses (e.g., Roden 1977, 1991; KR) that show the importance of surface Ekman convergence and differential surface fluxes to surface temperature frontogenesis in both the STFZ and SAFZ. Differential vertical mixing (as convective overturning) is an equally important process, particularly in the SAFZ, usually offsetting the effects of the other two processes. The balance between these three processes is also found to control the salinity frontogenesis. The importance of the convective overturning may explain why observational studies have had trouble identifying the dominant frontogenetic processes in the SAFZ. The shearing term is also important to the temperature and salinity frontogenesis in the model in the western part of the SAFZ. Observations support the peak temperature gradient in the western North Pacific SAFZ in winter (e.g., Roden 1980b and Fig. 1). However, the discrepancy in phase between the model and observations in the SAFZ in the central North Pacific requires further examination.

The seasonal cycle of the temperature, temperature gradient, and the temperature frontogenesis for the AVHRR SST climatology in the central Pacific (180° to 170°W) is shown in Fig. 13. The corresponding gradient and frontogenesis patterns from the model (lower-right and upper-left panels of Fig. 9) south of 40°N match the observations well. However, the seasonal cycle of frontogenesis/frontolysis at the location of the maximum temperature gradient in the model is much stronger than observed. The subarctic temperature front (SATF) in the model is at maximum strength during late winter/early spring while the AVHRR climatology shows peak strength during July/August. The magnitude and location of the maximum gradient of the SATF in the model during summer agree with observations, but the front is stronger and farther northward during winter.

In the model, the surface has cooled sufficiently near 40°N by December that temperatures are close to those at 100 m (creating the low stability gap discussed previously) (Fig. 13). Any further surface cooling (ignoring advection and diffusion) does little to lower the surface

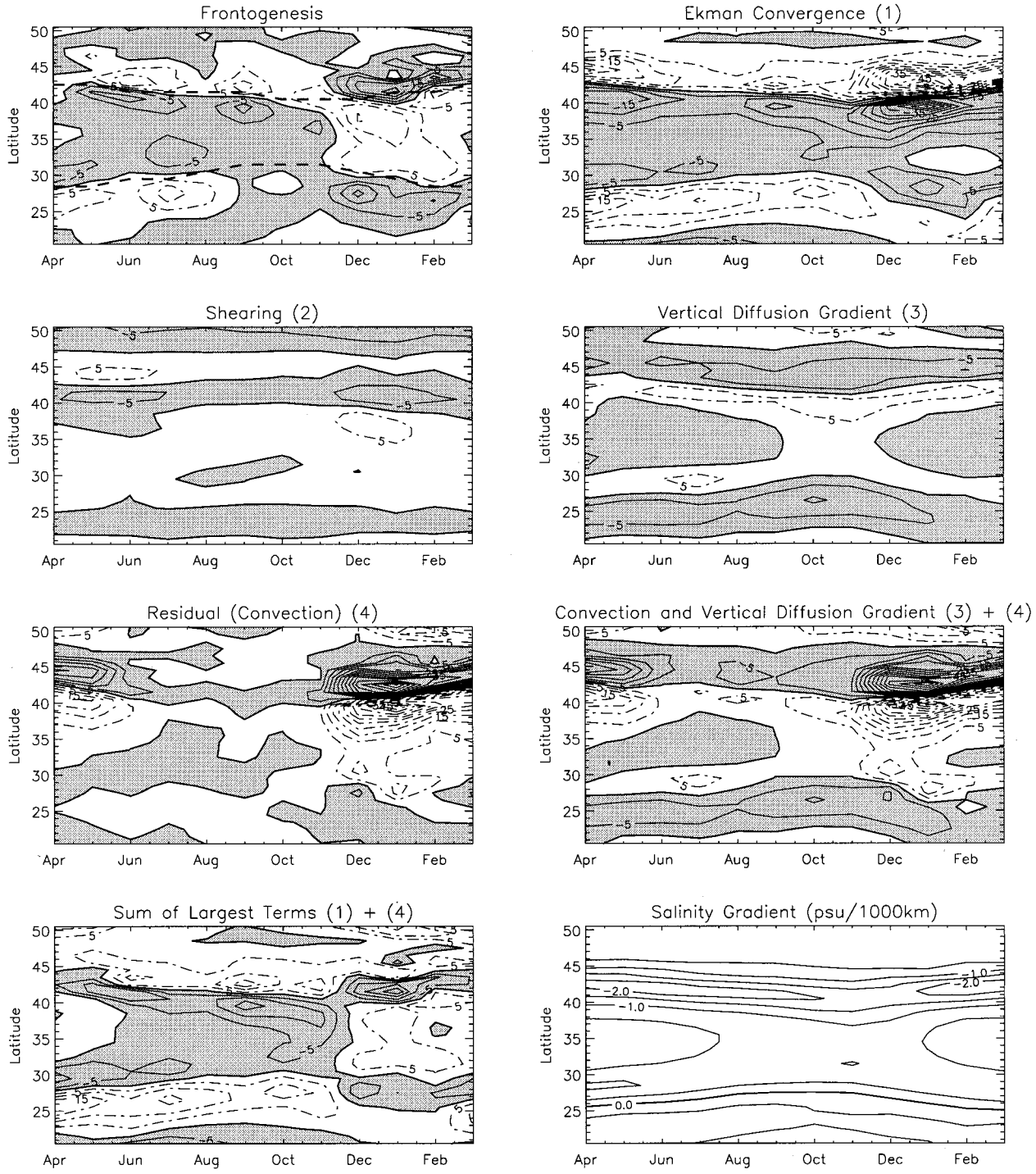

FIG. 12. As for Fig. 11 but for 180°–170°W at 5 m and with a contour interval of 5.0 for the frontogenesis panels.

temperature but instead initiates convective overturning. To the north and south where surface temperatures are higher than subsurface, the surface will continue to cool in response to the surface forcing. Thus, the gradient will increase to the north (frontogenesis) and decrease to the south (frontolysis) (e.g., top right-hand panel of Fig. 13). If the subsurface temperature is too high (say, because of the overshoot of the Kuroshio), the winter and spring frontogenesis/frontolysis associated with differential convection in this area will be exaggerated. However, it is still likely that this term is one of the dominant processes in the southern region of the SAFZ

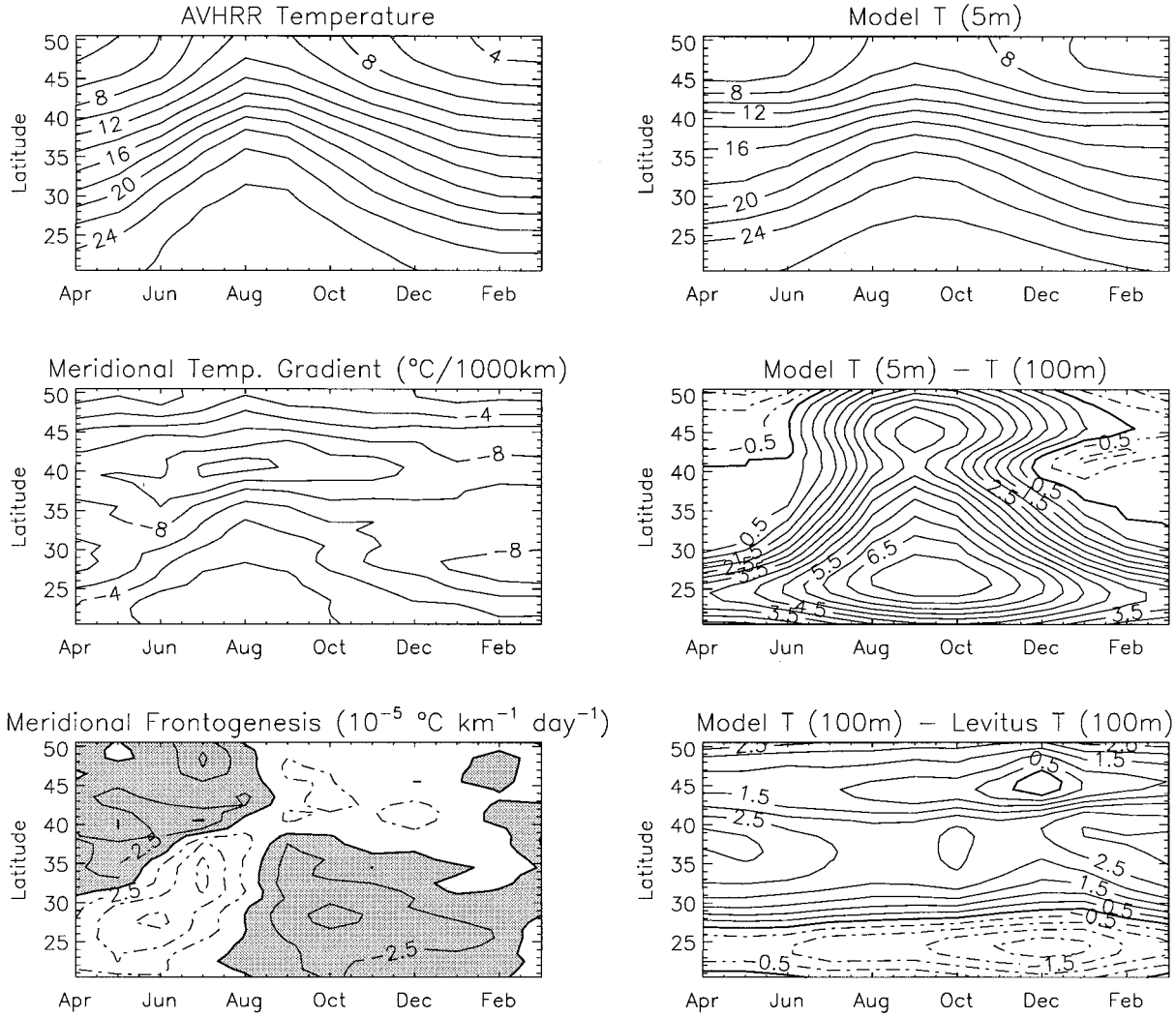

FIG. 13. (top left-hand panel) Monthly climatological AVHRR sea surface temperature as a function of latitude and time. (middle left-hand panel) Meridional AVHRR sea surface temperature gradient. (bottom left-hand panel) Frontogenesis from AVHRR data. (top right-hand panel) Monthly averaged model temperature at 5 m. (Middle right-hand panel) Monthly averaged model temperature at 5 m minus model temperature at 100 m. (bottom right-hand panel) Difference between monthly averaged model temperature and Levitus climatology temperature at 100 m. All plots are averages over the zonal band 180°–170°W.

because of the warm subsurface temperatures associated with the Kuroshio Extension. In the northern region of the SAFZ the effect of vertical convection is limited because of the strong, shallow halocline.

The location of the observed maximum temperature gradient in the central Pacific does not undergo as large a seasonal migration as in the model. However, the strength and phase of the temperature gradient at 40°N agree fairly well with observations (Fig. 9 cf. Fig. 13) as do the frontogenesis estimates at this latitude. In the meridional frontogenesis rate estimated from the AVHRR climatology (Fig. 13), the annual cycle at 40°N in the central SAFZ was weak, with a peak frontogenesis rate of 0.05°C/1000 km day^{-1} in July and a peak frontolysis rate of 0.04°C/1000 km day^{-1} in December. In comparison, the annual cycle in the southern part of the model SAFZ has a peak frontogenesis rate of 0.06°C/1000 km day^{-1} in July and a peak frontolysis rate of 0.05°C/1000 km day^{-1} in December. If the model processes at this latitude reflect those in the observed SAFZ, then the frontogenesis during spring and summer is due to surface Ekman convergence and horizontal shear. Frontolysis during fall is due to differential surface cooling. Frontolysis during winter is due to a balance between the frontolytic surface heat flux and differential vertical convection and the frontogenetic surface Ekman convergence.

6. Summary

The GFDL Modular Ocean Model, as configured for this experiment, simulates the location, strength, and

seasonal cycle of the OFZs in good agreement with observations. The SAFZ in the model contains relatively deep temperature and salinity high gradient regions that vary seasonally in strength but not much in position. The gradients are weaker in the eastern basin. The density gradient in the western portion of the SAFZ is strong (due to the close juxtaposition of the SAFZ and the Kuroshio Extension that has overshot its observed separation latitude) but is relatively weak throughout much of the SAFZ because of density compensation of the temperature and salinity fronts. The STFZ consists of a shallow region of high temperature gradient that disappears at the surface during summer/fall. The salinity front in the STFZ has less zonal variation in strength than the temperature front and more meridional variation in location. The region of high-density gradient extends across almost the entire basin.

The meridional temperature and salinity frontogenesis/frontolysis in the surface layer of the model is due primarily to the convergence of the wind driven Ekman transport, the differential surface fluxes, and (especially in the SAFZ) differential convective adjustment as a response to both surface convergence and surface cooling. Both temperature and salinity frontogenesis/frontolysis on seasonal timescales at 100 m in the western and central SAFZ are due primarily to differential mixing (mostly convective) and shearing advection associated with the western boundary current extension. In the STFZ in the central Pacific, Ekman convergence is the primary cause of the frontogenesis in the fall; vertical mixing and surface heating cause frontolysis during summer. Vertical mixing through convective adjustment in the model is a dominant process contributing to both frontogenesis and frontolysis. The large amount of vertical mixing shows the importance of the subsurface temperature field in determining the surface temperature frontogenesis/frontolysis. For the salinity field, the differential convection is primarily in response to meridional Ekman convergence and differential heat fluxes rather than freshwater fluxes, indicating the dependence of salinity frontogenesis on the temperature structure. The overshoot of the Kuroshio from its observed western boundary current separation latitude probably exaggerates the effects of differential vertical convection in the central SAFZ during winter and early spring. However, it is still likely that this term is one of the dominant processes throughout the SAFZ. At 40°N in the central basin, where the model seasonal cycle matches the observations well, the wintertime frontolysis is due to a balance between the frontolytic effect of surface heat flux and differential vertical convection and the frontogenetic effect of surface Ekman convergence.

These results highlight the importance of convective adjustment in the model (which does not include explicit mixed layer physics). The convection effectively extends the influence of surface heat and freshwater fluxes to below the first layer of the model. This is equivalent to a rapid increase in the mixed layer depth of a slab model. Kazmin and Rienecker (1996) used a slab mixed layer model to estimate the meridional frontogenesis in the central Pacific, and could not explain strong (typically 0.05°C/1000 km day^{-1} or greater) short-term (1–2 months) frontogenesis/frontolysis in the AVHRR data during winter–spring 1987–90 in the SAFZ. Kazmin and Rienecker (1996) noted that use of climatological values of the thickness of the mixed layer could be a potential source of error in their frontogenesis estimates. In the surface layer in the model used here (e.g., Figs. 8a, 9, 10), the largest values of R (which is dominated by convection) occur in winter–spring in the SAFZ and are very important in determining the total frontogenesis/frontolysis in the SAFZ. To simulate all the frontogenesis/frontolysis in a region and time where there is a large gradient in the surface cooling, explicit vertical turbulent mixing maybe necessary.

This study shows the relative importance of the shearing term to the temperature and salinity frontogenesis in the model in the western part of the SAFZ. The shearing term is frontogenetic throughout the year in the western part of the front and is important at the surface and even more so at depth. This term (which weakens rapidly as one moves eastward) is partially due to the model's representation of the Kuroshio Extension.

There are several improvements that could be made to this study. Finer horizontal resolution (eddy resolving) would certainly be useful in studying the effects of eddies on the frontogenesis and may be necessary for the inclusion of the smaller-scale effects in the daily winds. Niiler and Reynolds (1984) have suggested that deformation by the eddy field is important in synoptic frontogenesis. The model study of Bleck et al. (1988) suggests that the timescale of influence of the mesoscale deformation field would be about 3 days, compared with 30 days for the gyre-scale deformation field. Yuan (1994) has proposed that synoptic wind events may prove to be important to the maintenance of the SAFZ. This study suggests that such influence would be primarily through vertical mixing processes. Finer temporal resolution heat and freshwater fluxes that match the daily winds may also be necessary to study the smaller-scale effects of the winds properly. For example, Adamec and Garwood (1985) showed that surface buoyancy flux can impact the transient response of an upper-ocean density front to local wind events. A more accurate separation site for the Kuroshio would keep the Kuroshio front separate from the SAFZ and would certainly help to clarify some of the results. Preliminary results from a 1/4 degree model show a more realistic western boundary current separation. Finally, a more realistic model of the mixed layer physics would help to clarify the relative importance of wind-induced mixing and buoyancy convection, especially in the STFZ where the model mixed layer was too shallow.

Acknowledgments. The authors thank Troy Stribling for assistance with model configuration and plotting

packages and David Adamec for informative discussions and advice through the course of this study. The helpful comments from two reviewers are gratefully acknowledged. Much of this work was done while M.D. was a student supported through the Joint Center for Earth System Science in the Department of Meteorology at the University of Maryland. This project was funded by the NASA Physical Oceanography Program through the NASA RTOP 568-21-05.

REFERENCES

Adamec, D., and R. W. Garwood Jr., 1985: The simulated response of an upper-ocean density front to local atmospheric forcing. *J. Geophys. Res.,* **90,** 917–928.

Bingham, F. M., 1992: Formation and spreading of subtropical mode water in the North Pacific. *J. Geophys. Res.,* **97,** 11 177–11 189.

Bleck, R., R. Onken, and J. D. Woods, 1988: A two-dimensional model of mesoscale frontogenesis in the ocean. *Quart. J. Roy. Meteor. Soc.,* **114,** 347–371.

Camerlengo, A., 1982: Large-scale response of the Pacific Ocean subarctic front to momentum transfer: A numerical study. *J. Phys. Oceanogr.,* **12,** 1106–1121.

Cushman-Roisin, B., 1981: Effects of horizontal advection on upper ocean mixing: A case of frontogenesis. *J. Phys. Oceanogr.,* **11,** 1345–1356.

——, 1984: On the maintenance of the subtropical front and its associated countercurrent. *J. Phys. Oceanogr.,* **14,** 1179–1190.

daSilva, A. M., C. C. Young, and S. Levitus, 1995: *Atlas of Surface Marine Data* 1994. Vol. 1: *Algorithms and Procedures. NOAA Atlas NESDIS 7,* U.S. Department of Commerce, 74 pp.

ECMWF, 1994: The description of the ECMWF/WCRP level III-A global atmospheric data archive. Tech. Attach., Reading, England, 72 pp. [Available from ECMWF, Shinfield Park, Reading RG2 9AX, United Kingdom.]

Kazmin, A. S., and M. M. Rienecker, 1996: Variability and frontogenesis in the large-scale oceanic frontal zones. *J. Geophys. Res.,* **101,** 907–921.

Levine, E. R., and W. B. White, 1983: Bathymetric influences upon the character of North Pacific fronts. *J. Geophys. Res.,* **88,** 9617–9625.

Levitus, S., 1982: *Climatological Atlas of the World Ocean.* NOAA Prof. Pap. No. 13, U.S. Govt. Printing Office, Washington, D.C., 173 pp.

Lynn, R. J., 1986: The subarctic and northern subtropical fronts in the eastern North Pacific Ocean in spring. *J. Phys. Oceanogr.,* **16,** 209–222.

Niiler, P. P., and R. W. Reynolds, 1984: The three-dimensional circulation near the eastern North Pacific subtropical front. *J. Phys. Oceanogr.,* **14,** 217–230.

Pacanowski, R. C., 1995: MOM 2 documentation, user's guide and reference manual. GFDL Ocean Tech. Rep. No. 3, 232 pp. [Available from Geophysics Fluid Dynamics Laboratory, P.O. Box 308, Princeton, NJ 08542-0308.]

Qiu, B., 1995: Why is the spreading of the North Pacific Intermediate Water confined on density surfaces around σ_θ = 26.8? *J. Phys. Oceanogr.,* **25,** 168–180.

Roden, G. I., 1972: Temperature and salinity fronts at the boundaries of the subarctic–subtropical transition zone in the western Pacific. *J. Geophys. Res.,* **77,** 7175–7187.

——, 1975: On the North Pacific temperature, salinity, sound velocity and density fronts and their relation to the wind and energy flux fields. *J. Phys. Oceanogr.,* **5,** 557–571.

——, 1977: Oceanic subarctic fronts of the central Pacific: Structure of and response to atmospheric forcing. *J. Phys. Oceanogr.,* **7,** 761–778.

——, 1980a: On the subtropical frontal zone north of Hawaii during winter. *J. Phys. Oceanogr.,* **10,** 342–362.

——, 1980b: On the variability of surface temperature fronts in the western Pacific, as detected by satellite. *J. Geophys. Res.,* **85,** 2704–2710.

——, 1991: Subarctic–subtropical transition zone of the North Pacific: Large-scale aspects and mesoscale structure. NOAA Tech. Rep. NMFS 105, 1–38.

——, and D. F. Paskausky, 1978: Estimation of rates of frontogenesis and frontolysis in the North Pacific Ocean using satellite and surface meteorological data from January 1977. *J. Geophys. Res.,* **83,** 4545–4550.

Smith, E., 1992: A user's guide to the NOAA advanced very high resolution radiometer multichannel sea surface temperature data set produced by the University of Miami/Rosenstiel School of Marine and Atmospheric Science. JPL Tech. Rep. 037-D001, Jet Propulsion Laboratory, Pasadena, CA, 22 pp. [Available from JPL Archives and Records Management Facility, Sherikon Space Systems, Inc., 145 N. Aldena Drive, Pasadena, CA 91107.]

Suga, T., Y. Takei, and K. Hanawa, 1997: Thermostad distribution in the North Pacific subtropical gyre: The central mode water and the subtropical mode water. *J. Phys. Oceanogr.,* **27,** 140–152.

Takeuchi, K., 1984: Numerical study of the subtropical front and the subtropical counter-current. *J. Oceanogr. Soc. Japan,* **40,** 371–381.

——, 1986: Numerical study of the seasonal variations of the subtropical front and the subtropical countercurrent. *J. Phys. Oceanogr.,* **16,** 919–926.

Trenberth, K. E., W. G. Large, and J. E. Olson, 1989: The effective drag coefficient for evaluating wind stress over the oceans. *J. Climate,* **2,** 1507–1516.

Tziperman, E., J. R. Toggweiler, Y. Feliks, and K. Bryan, 1994: Instability of the thermohaline circulation with respect to mixed boundary conditions: Is it really a problem for realistic models? *J. Phys. Oceanogr.,* **24,** 217–232.

White, W. B., K. Hasunuma, and H. Solomon, 1978: Large-scale seasonal and secular variability of the subtropical front in the western North Pacific from 1954 to 1974. *J. Geophys. Res.,* **83,** 4531–4544.

Yuan, X., 1994: Characteristics and frontogenesis of the subarctic front in the North Pacific. Ph.D. dissertation, University of California, San Diego, 172 pp.

——, and L. D. Talley, 1996: The subarctic frontal zone in the North Pacific: Characteristics of frontal structure from climatological data and synoptic surveys. *J. Geophys. Res.* **101,** 16 491–16 508.

Zhang, R.-C., and K. Hanawa, 1993: Features of the water-mass front in the northwestern North Pacific. *J. Geophys. Res.,* **98,** 967–975.